WADD-TR-61-72
VOLUME XXXIX

RESEARCH AND DEVELOPMENT ON ADVANCED GRAPHITE MATERIALS

VOLUME XXXIX. DIAMAGNETIC SUSCEPTIBILITY OF GRAPHITE BY THE FARADAY METHOD

TECHNICAL DOCUMENTARY REPORT No. WADD-TR-61-72, VOL. XXXIX

NOVEMBER 1963

AF MATERIALS LABORATORY
AERONAUTICAL SYSTEMS DIVISION
AIR FORCE SYSTEMS COMMAND
WRIGHT-PATTERSON AIR FORCE BASE, OHIO

Project No. 7350, Task No. 735002
Project No. 7381, Task No. 738102
Project No. 7-817

NOTICES

When Government drawings, specifications, or other data are used for any purpose other than in connection with a definitely related Government procurement operation, the United States Government thereby incurs no responsibility nor any obligation whatsoever; and the fact that the Government may have formulated, furnished, or in any way supplied the said drawings, specifications, or other data, is not to be regarded by implication or otherwise as in any manner licensing the holder or any other person or corporation, or conveying any rights or permission to manufacture, use, or sell any patented invention that may in any way be related thereto.

Qualified requesters may obtain copies of this report from the Defense Documentation Center (DDC), (formerly ASTIA), Cameron Station, Bldg. 5, 5010 Duke Street, Alexandria 4, Virginia

This report has been released to the Office of Technical Services, U.S. Department of Commerce, Washington 25, D.C., in stock quantities for sale to the general public.

Copies of this report should not be returned to the Aeronautical Systems Division unless return is required by security considerations, contractual obligations, or notice on a specific document.

900 - December 1963 - 162-21-353

FOREWORD

Other reports issued under USAF Contract AF 33(616)-6915 have included:

WADD Technical Notes 61-18 and 61-18, Part II, progress reports covering work from the start of the contract on May 1, 1960, to October 15, 1961, and the following volumes of WADD Technical Report 61-72, covering various subject phases of the work:

Volume I	Observations by Electron Microscopy of Dislocations in Graphite, by R. Sprague.
Volume II	Application of Anisotropic Elastic Continuum Theory to Dislocations in Graphite, by G. B. Spence.
Volume III	Decoration of Dislocations and Low Angle Grain Boundaries in Graphite Single Crystals, by R. Bacon and R. Sprague.
Volume IV	Adaptation of Radiographic Principles to the Quality Control of Graphite, by R. W. Wallouch.
Volume V	Analysis of Creep and Recovery Curves for ATJ Graphite, by E. J. Seldin and R. N. Draper.
Volume VI	Creep of Carbons and Graphites in Flexure at High Temperatures, by E. J. Seldin.

ABSTRACT

The diamagnetic susceptibility of several types of graphite, both single and polycrystalline, was investigated at room temperature by the Faraday method. This method measures the entire sample; it can be used to obtain the three components for a trace; and it can account for ferromagnetic impurities. For single crystals, the conduction electron component ($\parallel$ c-axis) is $\chi_\parallel = -21.8 \times 10^{-6}$ emu/gm; whereas the isotropic ionic core component is $\chi_\perp = -0.32 \times 10^{-6}$ emu/gm, resulting in a maximum anisotropy ratio of 68. (Anisotropies found for polycrystals range from 25 for annealed pyrolytic down to 1.01 for lampblack-base grade CEP graphite. The susceptibility trace, representing the contribution of the truly graphitic portion of a sample, ranges from -22.8×10^{-6} emu/gm for single crystals down to -19.1×10^{-6} emu/gm for grade ZTA graphite) Direct orientation measurements showed that both single crystals and polycrystals display a true cosine-squared dependence, modified in amplitude by the degree of preferred crystallite orientation. These results are justified theoretically.

A study of the effect of annealing temperature up to 3360 °C on the anisotropy and trace of pyrolytic samples showed a competition of processes depending upon the properties of the "as received" material, where trace values vary from -18.2×10^{-6} emu/gm to -24.0×10^{-6} emu/gm according to the amount of non-graphitic carbon and the degree of turbostraticity. (Above ~ 3200 °C, all sample traces tend toward the single crystal value.)

A study of the effect of acceptor boron doping from 1 to 5000 ppm showed a decrease in the magnitude of $\chi_\parallel$ with increasing boron concentration, following the lowering of the Fermi level, becoming asymptotic to the ionic core component at $\sim 3 \times 10^{-3}$ B/C. This effect correlates with the Hall coefficient, which shows a peak due to the transition at the bottom of the conduction band from mixed conduction to single hole conduction. Both effects give an ionization efficiency for boron of $75 \pm 15\%$. Magnetoresistance and conductivity results show that there is predominantly impurity scattering in the measured range of 77 °K to 299 °K.

This report has been reviewed and is approved.

W. G. RAMKE
Chief, Ceramics and Graphite Branch
Metals and Ceramics Division
Air Force Materials Laboratory

TABLE OF CONTENTS

TABLE OF CONTENTS (Cont.)

LIST OF TABLES

LIST OF ILLUSTRATIONS

1. INTRODUCTION

The purpose of this investigation is to gain information about graphite single crystal properties from which an extension can be made to related properties of fabricated polycrystalline graphites. The magnetic susceptibility can give direct information about the electronic properties such as the Fermi level position, carrier concentration, and crystalline defect structure. These properties are common to both single and polycrystalline samples since the susceptibility is relatively independent of electron scattering--a complication in the interpretation of galvanomagnetic and transport measurements. The problem is, then, one of transferring the individual components of the reasonably well understood single crystal to a matrix of similar crystallites forming a polycrystalline sample. The Faraday method was chosen as the most suitable approach for this study because it can be used to accurately measure the entire susceptibility throughout a sample; it can be used to account for ferromagnetic impurities; and it can measure the three individual orthogonal components, the sum of which is the susceptibility trace. A ratio of two of these components gives the anisotropy, which is extremely large in single crystals and which gives the degree of crystallite orientation in polycrystals. The susceptibility trace of a polycrystal when compared to that of a single crystal gives the contribution of the truly graphitic portion of a sample and can thus be used in a study of lattice defects. In addition, certain ionized impurities shift the Fermi level, thereby affecting the susceptibility trace. In this report, the first section is devoted to a discussion of the Faraday method and apparatus; the second considers the susceptibility trace, anisotropy, and orientation dependence of pure single and polycrystalline graphites; the third deals with the susceptibility dependence of pyrolytic graphite upon annealing temperature; and the last section covers the behavior of the susceptibility with boron doping.

2. SUMMARY

2.1. Method of Measurement

The Faraday method of measuring magnetic susceptibility is the most suitable one because it measures the entire susceptibility throughout a sample, can be used to measure three orthogonal directions for the trace, and can account for ferromagnetic impurities. An apparatus employing this technique was constructed using specially shaped pole pieces to produce a constant H dH/dz region in which the sample is placed. A quartz microbalance having a "least count" under operating conditions of 0.5 µg was used to detect the small forces involved giving an overall accuracy for the susceptibility measurement of ± 1 per cent. It was operated in the magnetic field range from 10 to 22 kilogauss to allow corrections to be made for ferromagnetic impurities by the Honda-Owen method. Different representative types of graphite have been measured including single crystals, both natural and synthetic, several types of pyrolytic, and grades ZTA, AGK-SP, CEP, ATJ, and L113SP. The single crystals were in the form of small platelets 1 to 3 mm in diameter by 0.1 to 0.3 mm thick and the polycrystalline samples were cut into cubes 0.050 inch on a side to facilitate measurements in three perpendicular directions for trace values. Special suspensions were designed to restrict the sample from rotating in the magnetic field without contributing unduly to the measured value itself, in order to meet the requirements of the small size and high anisotropy of the samples.

2.2. Orientation Dependence of Magnetic Susceptibility of Graphite

A careful study has been made of the anisotropy of the various forms of graphite by a direct observation of the orientation dependence. For the highly anisotropic single crystals, the component $\chi_{\parallel}$ parallel to the hexagonal axis averages -21.8×10^{-6} emu/gm and is due almost entirely to the conduction electron contribution. The isotropic component $\chi_{\perp}$ in the basal plane, due to the ionic core electrons, was found to have a value of -0.32×10^{-6} emu/gm. This value for the ionic core component was determined by taking into account the orientation and degree of twinning of individual crystals in a direct way. For polycrystalline materials the anisotropy is much less. For example, the values of $\chi_{\parallel}/\chi_{\perp}$ range from 41 to 76 for single crystals and from 9 to 22 for pyrolytic graphites and are 2.1 for grade ZTA, 1.9 for grade AGK-SP, 1.3 for grade ATJ, 1.02 for grade L113SP, and 1.01 for grade CEP graphite. It has been found for the first time by direct experimental observation that the orientation dependence of the susceptibility of both single crystals and polycrystalline graphites exactly obeys the theoretical cosine-squared relation. The magnitude of the angular variation of the susceptibility for polycrystalline materials measures the degree of preferred orientation of the crystallites in these materials.

2

2.3. Trace of Magnetic Susceptibility of Graphite

The susceptibility trace (sum of three perpendicular components) is invariant to a rotation of the measurement axes and, hence, is the same for a pure material in both the single crystal and polycrystalline forms. The susceptibility trace for single crystals was found to have the value -22.8×10^{-6} emu/gm. The range of trace values measured on polycrystalline graphites runs from -21.6×10^{-6} emu/gm for heat-treated pyrolytic to -19.1×10^{-6} emu/gm for grade ZTA. The decrease of the magnitude of the polycrystalline trace values of up to 16 per cent below the single crystal value is due to small fractions of the sample that may be composed of non-graphitic carbon, of microcrystals less than ~ 150 Å in size, and of impurities. However, a section of the sample might have the rhombohedral (abcabc stacking scheme) modification or the two-dimensional turbostratic structure. In this case, since both of these structures have a theoretical trace susceptibility value of about -39×10^{-6} emu/gm, this contribution would actually increase the measured trace.

2.4. Effect of Annealing on Magnetic Susceptibility of Pyrolytic Graphite

The effect of annealing temperatures from 2000° to 3360°C upon the susceptibility trace and anisotropy have been investigated on three specimens of pyrolytic graphite with deposition temperatures between 2000° and 2100°C. In addition, lattice spacings were measured concurrently on identical samples by X-rays. In general, an increase in $\chi_{\parallel}$ and a decrease in $\chi_{\perp}$ were observed; this result was caused by the partial annealing which flattened the layer planes. The resulting change in the anisotropy runs from 7 to 20 for the best pyrolytic sample investigated. With increasing annealing temperature the behavior of the susceptibility trace reflects the competition between two processes: (a) the further graphitization of remaining non-graphitic carbon, as indicated by the observed growth in crystallite size which increases the magnitude of the trace, and (b) the transformation from a turbostratic two-dimensional structure to an ordered three-dimensional hexagonal structure, which decreases the magnitude of the trace.

2.5. Effect of Doping on Susceptibility of Graphite

Artificial graphites contain imperfections which both shift the Fermi level and change the band structure. As a preliminary step in studying naturally occurring imperfections, doping studies have been made on both natural and artificial graphites. Controlled doping has been used to change the Fermi level by known amounts without markedly changing the band structure. General agreement has been found between theory and experiment.

The behavior of the diamagnetic susceptibility of three types of graphite (L113SP, AGK-SP, and single crystals) was investigated as a function of boron content in the range of 1 ppm up to 6000 ppm. Although this series of samples represents cyrstallite sizes from ~ 300 A to ~ 2 mm and anisotropy

3

ratios from 1.02 to about 50, the relative behaviors are basically the same. The trace χ_T shows a strong shoulder on a semi-log plot in the range from $\sim 10^{-4}$ to $\sim 3 \times 10^{-3}$ B/C atom ratio, changing from its pure graphite value to $\sim 2 \times 10^{-6}$ emu/gm and becoming asymptotic to the isotropic boron insensitive component $3\chi_{ion\ core}$. This shoulder is due to the rapid decrease of the large boron sensitive component $\chi_{conduction}$ as the Fermi level shifts through the band overlap region toward a p-type behavior governed by the acceptor boron. A reasonable agreement between the single crystal results and the theory of McClure is obtained by assuming an ionization efficiency of 75 ± 15 per cent. This figure was also arrived at independently by applying the two-band model to the Hall effect results, where a maximum was observed in the same region corresponding to the transition from a mixed electron and hole conduction to that of hole conduction alone. Boron was chosen as a nearly ideal acceptor because of its small size (0.4 A diameter of the B^{+3} ion compared to the nearest-neighbor spacing in the graphite lattice of 1.42 A) and because it has one less valence electron than carbon. Although X-ray determinations show a slight distortion of the lattice, and the electrical conductivity shows an increase in the electron scattering, this study demonstrates that the susceptibility is a good indicator of the intrinsic shift of the Fermi level occurring within the crystallites, regardless of the macroscopic graphite type.

3. FARADAY METHOD FOR MEASUREMENT OF MAGNETIC SUSCEPTIBILITY

The magnetic susceptibility is related directly to electronic properties common to both the single and polycrystalline forms of a material. As a means of measuring the susceptibility, the Faraday method is most suitable, though difficult, because it measures the entire susceptibility throughout a sample, can be used to measure three orthogonal directions for the trace, and can account for ferromagnetic impurities. To see what would be required in such a measurement, let us first consider the relation between the susceptibility of a material and the resultant force in a magnetic field. In free space, the energy due to a magnetic field is

$$E = \tfrac{1}{2} \int \underline{B} \cdot \underline{H} \, dv = \frac{\mu_0}{2} \int H^2 \, dv. \tag{1}$$

When a sample material with a finite volume susceptibility, K_s (dimensionless), and permeability, $\mu_s = \mu_0 (K_s + 1)$, is inserted into a medium having values K_m and μ_m, the excess energy introduced is

$$\Delta E = \frac{\mu_0}{2} \int (K_s - K_m) H^2 \, dv, \tag{2}$$

where the integral is taken over the volume of the sample. For example, K_m may refer to free space where it equals zero or to air where[1] $K_m = 2.52 \times 10^{-3}/T^2$, T being the absolute temperature. At 299 °K this value is $+0.028 \times 10^{-6}$.

In general, K_s is anisotropic and so must be put in tensor form giving for the sample contribution

$$\Delta E_s = \frac{\mu_0}{2} \int [\, K_{11}H_x^2 + K_{22}H_y^2 + K_{33}H_z^2 + 2K_{12}H_xH_y + 2K_{23}H_yH_z + 2K_{31}H_zH_x \,] \, dv . \tag{3}$$

This equation may be simplified, however, since a real substance has three mutually perpendicular, principal magnetic axes[2] having the property $K_{12} = K_{23} = K_{31} = 0$ and for which the associated principal susceptibilities are $K_1 = K_{11}$, $K_2 = K_{22}$, and $K_3 = K_{33}$. Thus, equation (3) reduces to

$$\Delta E_s = \frac{\mu_0}{2} \int [\, K_1 H_x^2 + K_2 H_y^2 + K_3 H_z^2 \,] \, dv . \tag{4}$$

In the Faraday method, the entire relatively small sample is placed in a magnetic field gradient and the force exerted on the sample transverse to the field is measured. If H is in the x-direction, then the force in the z-direction is given by

$$F_z = \frac{d}{dz} \Delta E. \tag{5}$$

Providing that the sample is magnetically homogeneous, that H is sensibly constant throughout the volume of the sample, and that $H_y = H_z = 0$, the force in dynes is

$$F_z = \mu_0 v (\kappa_s - \kappa_m) H_x \frac{dH_x}{dz} = \mu_0 m (\chi_s - \chi_m) H_x \frac{dH_x}{dz} \quad , \qquad (6)$$

where, with ρ the density, the mass susceptibility is $\chi = \kappa/\rho \cong [\,cm^3/gm\,]$. These units for χ are commonly expressed in the literature, however, as emu/gm. To avoid confusion, the latter unit also will be adopted throughout this paper. In equation (6), m is in gm, H in oersted, and z in cm.

In a true experimental situation, certain qualifications should be made concerning some of the assumptions used in evaluating equation (6). Essentially, it is a question of the uniformity of H_x and H_z over the sample volume and the magnitude of the anisotropy ratio, χ_1/χ_3. In effect, one has in the force equation the sum of two terms

$$\chi_1 H_x \frac{dH_x}{dz} \qquad + \qquad \chi_3 H_z \frac{dH_z}{dz}$$

to integrate over the sample volume, and in some cases the contribution of the second term may indeed be sizable. The quantity $H_x dH_x/dz$ must be made as constant as possible over a usable sample volume. Special pole pieces, designed by Donoghue[3] according to the theory of Davy,[4] produce equipotential surface contours bounding the air gap given by $r^{3/2} \sin(3\phi/2) =$ constant, where the origin is a central point in the air gap and r is the radius vector to the pole-piece surface and oriented at an angle ϕ from the vertical as shown in Figure 1. This cross section is constant as viewed along the y-axis, which is normal to the paper. A family of experimentally determined
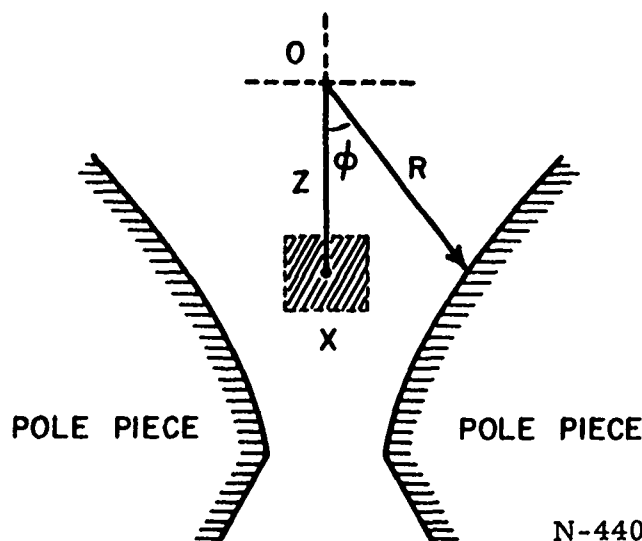
Figure 1. Pole-piece Configuration Given by
$r^{3/2} \sin(3\phi/2) =$ Constant.

6

$H_x dH_x/dz$ curves versus z for different magnetic currents obtained with this pole configuration is shown in Figure 2. The depth, z, is given as the
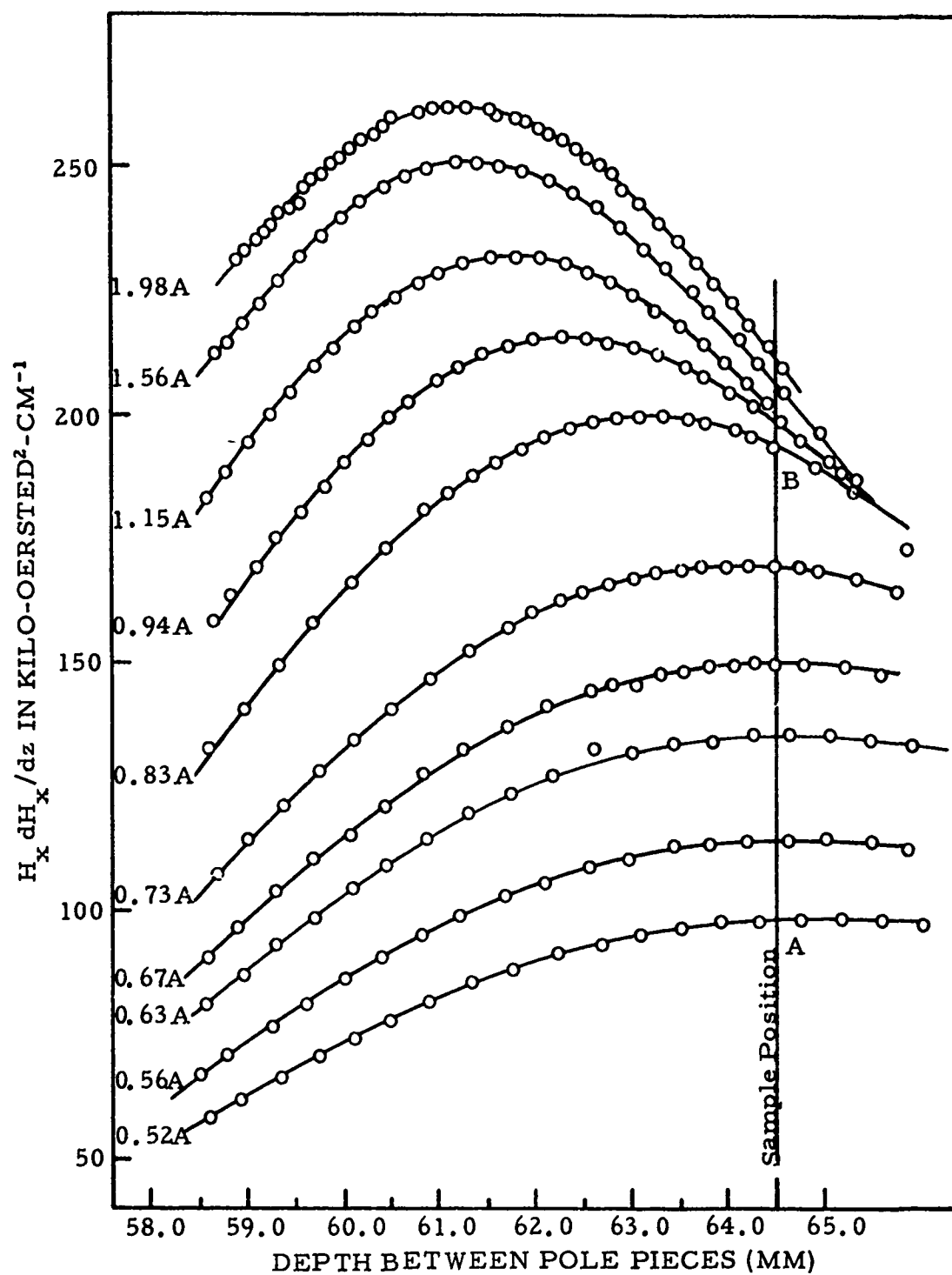
Figure 2. $H_x dH_x/dz$ Curves Versus Depth.

N-4404

7

distance to a fixed fiducial mark on the apparatus (top of the pole-piece housing flange). This process of sample location was an extremely critical one and much time was spent in perfecting the technique. A sample could be located with a cathetometer to within ±0.02 mm. The breadth of the samples ranged from about 1-4 mm, although most samples were less than 2 mm. For example, the best single crystals were between 1.2 and 2 mm whereas the polycrystalline cubes were cut to 1.3 mm on a side. For the largest crystal diameter of 4 mm, a maximum error in $H_x dH_x/dz$ of 1.3 per cent is involved. For most of the samples, however, this error would be negligible.

The corresponding magnetic field at the sample position is given for the same magnet currents in Figure 3. A Varian 4-inch electromagnet with a
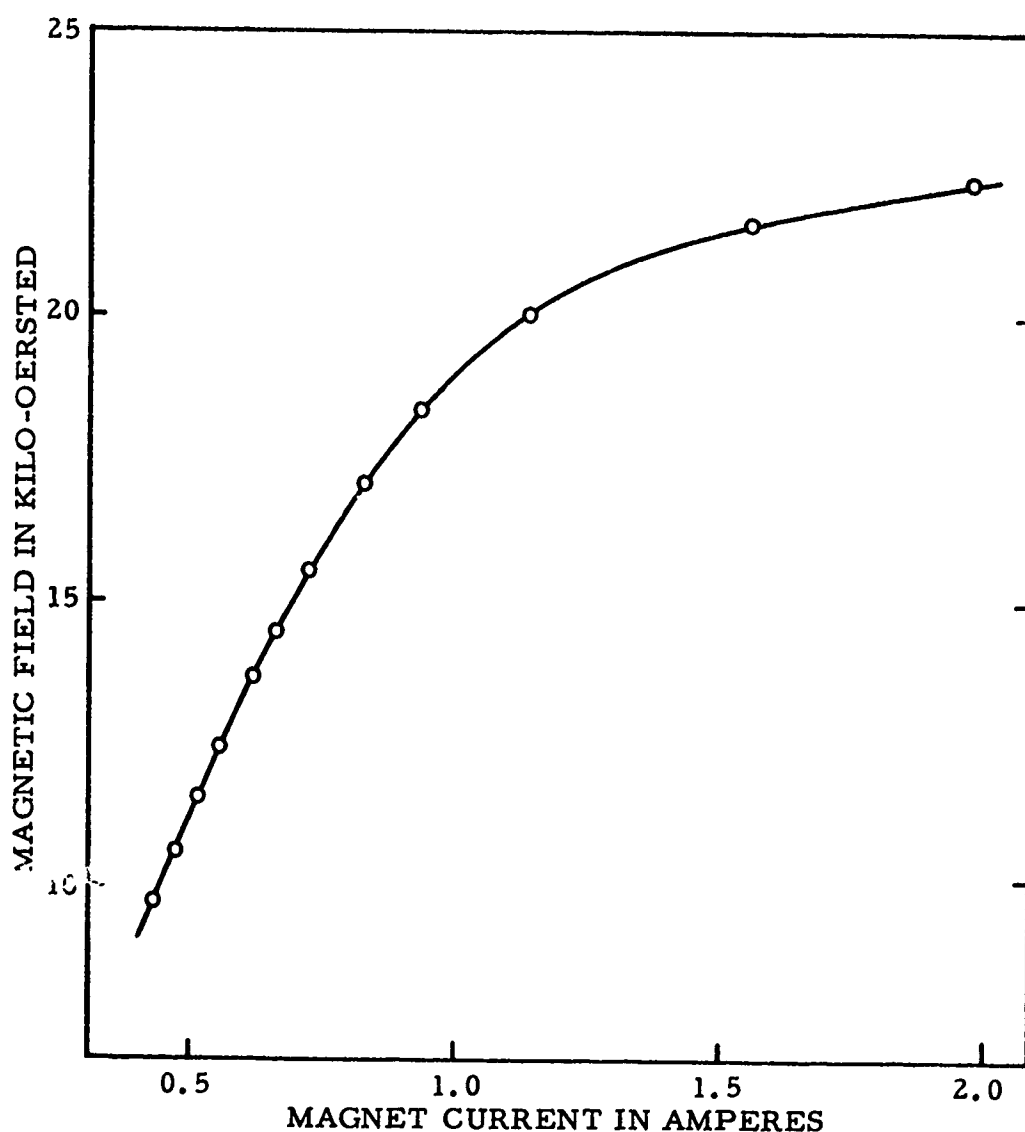
Figure 3. Magnetic Field at Sample Position

N-4405

8

power supply, stabilized to 1 part in 10^4 as designed in this laboratory, provided the field. This supply is shown schematically in Figure 4.
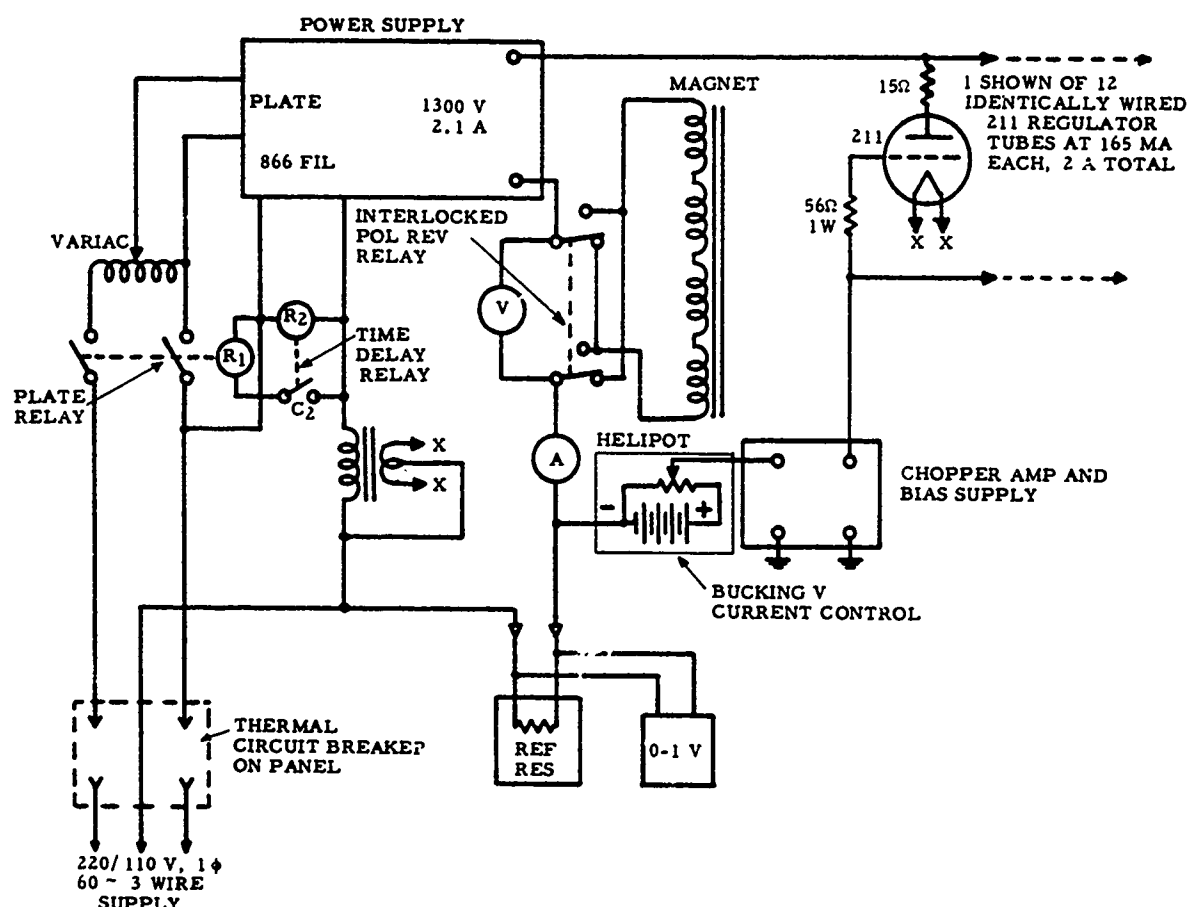
N-4406

Figure 4. Magnet Power Supply Schematic Diagram.

A cryostat was incorporated in the apparatus enabling measurements to be made from 83 °K up to 660 °K. Since this feature has been perfected recently, only room temperature results made in air are reported here. Because of the small space restrictions between the pole pieces, the latter were situated within the vacuum space of the cryostat as shown in Figure 5.
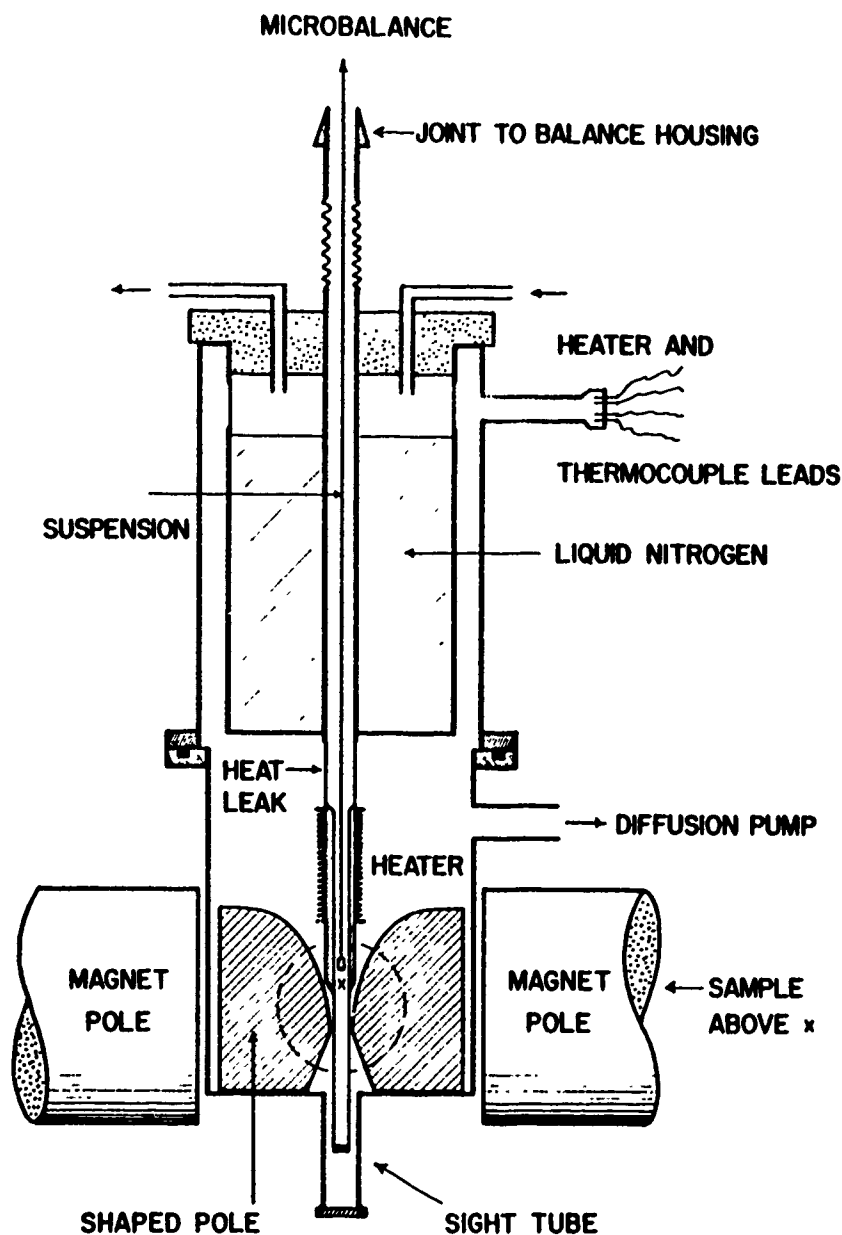
N-4407

Figure 5. Susceptibility Cryostat with Shaped Pole Pieces

A sight tube located at the bottom allowed us to locate the sample in the inner vacuum space. The front window (shown by the dashed circles in the diagram) allowed us to maintain the spacing (~ 0.002-inch) between the sample housing tube (1/8-inch O.D.) and the pole pieces.

A quartz microbalance, designed and built by A. W. Czanderna,[5] was used to detect the small forces encountered. This balance is shown along with the cryostat, magnet, and power supply in the overall picture of the apparatus in Figure 6. A split "D" type electromagnetic coil is used to maintain a null balance by acting upon a small nickel wire mounted on the beam itself. A second identical nickel wire is mounted symmetrically on the other side of the fulcrum to compensate for stray magnetic fields from the main magnet. Under operating conditions, this arrangement has a least count of ± 0.5 μgm, resulting in an error from this part of the apparatus of less than one per cent.

New suspension techniques had to be devised because of graphite's extreme anisotropy and exceedingly small crystal size. For a general orientation dependence (see Section 2 for a discussion), the crystal had to be constrained by a rigid but light suspension with a low susceptibility while the magnet was rotated on its trunnion mount. A copper tube 1/16-inch in diameter having a 0.003-inch wall (χ = -0.086 x 10^{-6} emu/gm) and a precisely flattened tip was suspended from the quartz balance arm. The single crystal or polycrystalline cube was held securely against the flat portion with a small dab of stopcock grease. The suspension plus grease was always pre-checked for its contribution.

Though reasonable measurements of $\chi_\perp$, the component perpendicular to the c-axis in graphite, could be made with the copper suspension, such a suspension was a limiting factor with very small samples. A check was made by another more precise method that consisted of straddling a ... tal between two flexible Teflon monofilaments (χ = -0.3 x 10^{-6} emu/gm a. ~0.0005-inch diameter) suitably held in place with relatively loose slip knots and counterweighted by a small copper hook that hung well out of the magnetic field. This procedure permitted the crystal to orient itself in the magnetic field exactly to the minimum orientation with an almost negligible contribution from the suspension. Even so, this latter contribution was carefully determined before and after each measurement. Even such effects as the perspiration from one's hand could contribute a detectable effect. Typical sets of data taken on the graphite single crystal, EP-58, for both of the $\chi_\perp$ components with the Teflon monofilament suspension are shown in Table 1.

Ordinary diamagnetic and paramagnetic impurities (see Section 4, p. 18) of a few parts per million concentration contribute a negligible effect. Ferromagnetic impurities, however, are extremely important factors for they may contribute forces of 10^4 to 10^5 times greater. Consider the measured or apparent susceptibility, χ^*, as obtained from equation (6). A ferromagnetic impurity contributes an additional force term, which is related to χ^* and the true sample susceptibility, χ, by

11
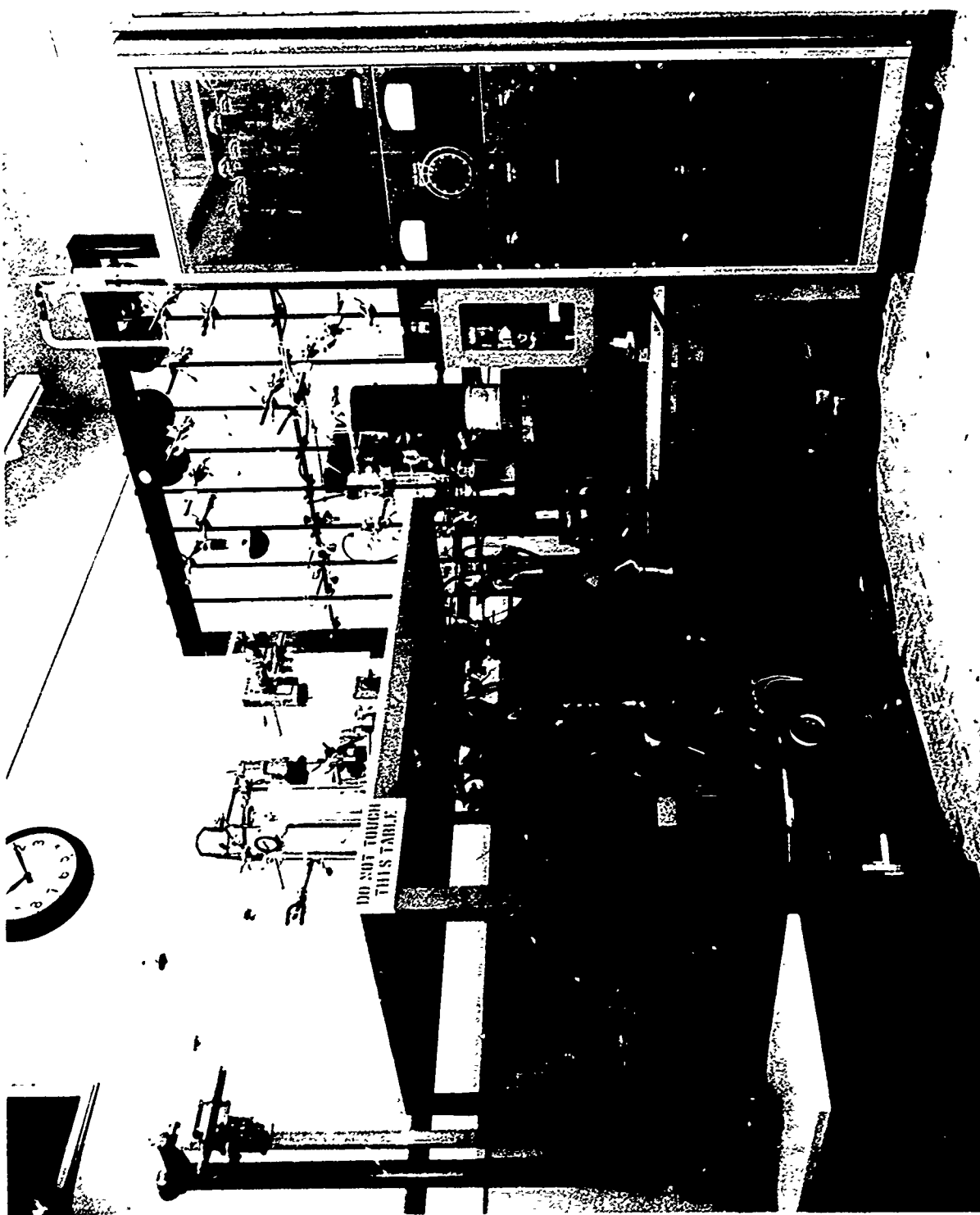
Figure 6. View of Entire Susceptibility Apparatus   U-1579

Table 1. Typical $\chi_\perp$ Data for Graphite Crystal EP-58 Showing
the Teflon Suspension Contribution
m = 0.656 ± 0.002 milligram

Magnetic Field (kilo-oersted)	Suspension Contribution (%)	Apparent Susceptibility (10^{-6} emu/gm)
$\chi_{\perp_1}$		
20.0	39.4	-0.359
18.4	30.4	-0.348
17.1	25.1	-0.353
15.6	23.1	-0.348
14.5	22.5	-0.355
13.7	20.3	-0.361
12.5	20.5	-0.363
11.6	21.6	-0.366

Average $\chi_{appar.}$ = -0.357 ± 0.006 x 10^{-6} emu/gm

$\chi_{\perp_2}$		
20.0	43.1	-0.329
18.4	31.7	-0.334
17.1	27.6	-0.321
15.6	24.0	-0.335
14.5	24.5	-0.326
13.7	21.9	-0.335
12.5	22.2	-0.335
11.6	23.0	-0.343

Average $\chi_{appar.}$ = -0.332 ± 0.004 x 10^{-6} emu/gm

$$\chi^* = \chi + \frac{m(Fe)}{m(sample)} \frac{M_s(Fe)}{H} \tag{7}$$

where m is the mass and M_s(Fe) is the saturation magnetization per gram (217 emu/gm) of the ferromagnetic impurity.[6] Thus, where measurements are made as a function of H in a sufficiently high range to saturate these impurities, a plot of χ^* versus 1/H would be a straight line with a slope of m(Fe) M_s(Fe)/m(sample) and with an intercept of χ at H = ∞. This is the Honda-Owen[7,8] method, representing one of the unique features of the Faraday type of measurement. With our apparatus, measurements could be made in the 10 to 22 kilo-oersted range; however, the most accurate range employed was from 11.6 to 17.1 kilo-oersteds, as shown by the region between A and B in Figure 2.

Calibration was first carried out in an absolute way using a specially designed flip coil with a diameter of 1.78 mm constructed of 2275 turns of 0.001-inch constantan wire having a resistance of 7300 ohms. This coil was calibrated against proton resonance. The H dH/dz curves in Figure 1

13

were taken both with this coil and later with a 2.18 mm diameter pure silver sphere to give the resultant force on the microbalance directly. Honda-Owen plots taken on pure Au, Ag, and Cu are shown in Figure 7. Our
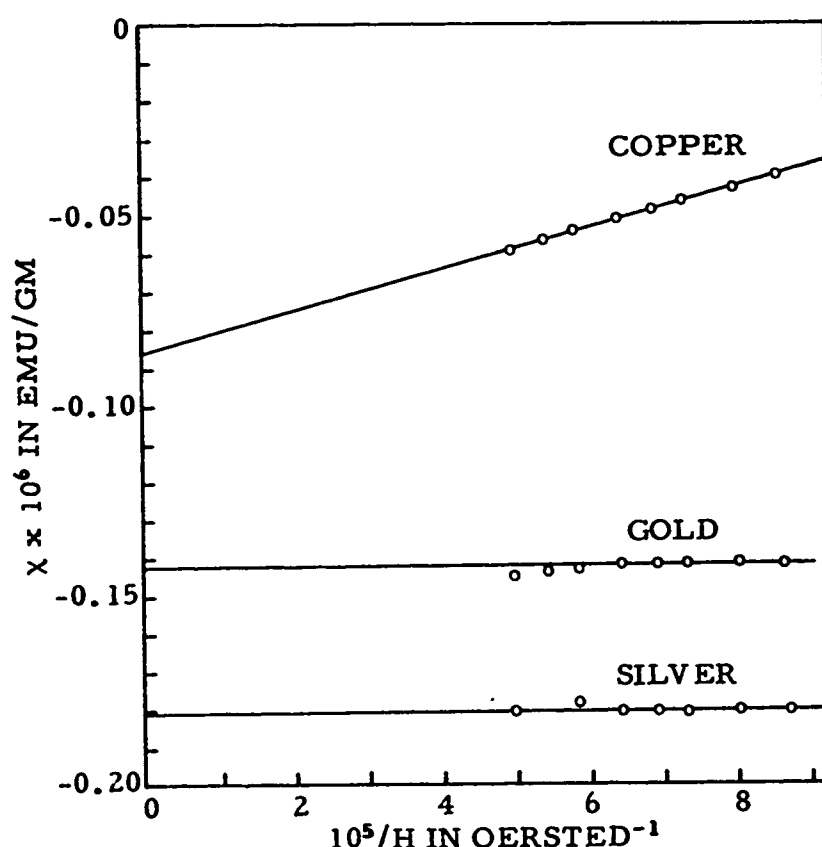
Figure 7. Honda-Owen Plots of N-4408
Copper, Silver, and Gold.

calibration was compared to the well established values shown in Table 2.

Table 2. Susceptibility Calibration Values for Copper,
Silver, and Gold. (Units of 10^{-6} emu/gm)

| Metal | Faraday | | Guoy | Standard Reference Value | Reference |
	Flipcoil	Standard			
Gold	-0.140±0.002	-0.143	-0.141±0.004	-0.142	9 and 10
Silver	-0.175±0.005	-0.181*	-----	-0.181	9, 10 and 11
Copper	----	-0.085	-0.086±0.003	-0.086	9, 10 and 12

*Set as reference standard.

The flip coil value for Au, the most reliable, was 1.4 per cent low. To improve the calibration, we chose silver as a secondary standard ($-0.181 \pm 0.001 \times 10^{-6}$ emu/gm) since its susceptibility is almost independent of temperature. We used small pure silver spheres which were ideal for this purpose, both because of their shape and because no cutting or shaping was necessary, thereby avoiding contamination. Such a sample made a convenient means of checking and maintaining calibration of the entire apparatus under operating conditions. Later, as a matter of interest, we made an additional independent check by measuring pure Au and Cu samples on a Guoy balance. These results are also shown in Table 2. The overall error with this Faraday apparatus is approximately one per cent.

4. DIAMAGNETIC SUSCEPTIBILITY OF PURE GRAPHITE

The diamagnetic susceptibility of graphite has been studied for a long time by different methods and from different points of view. Its most striking features are its very large* component in the direction of the hexagonal axis, $\chi_{\parallel}$, and its small component, $\chi_{\perp}$, isotropic in the basal plane. This large, almost two-dimensional anisotropy, is related directly to graphite's hexagonal layer-type crystal structure. There is tight covalent bonding between adjacent atoms within a plane (1.42 Å spacing) and rather loose van der Waal-type bonding between planes (3.35 Å spacing). The large magnitude of $\chi_{\parallel}$ is due qualitatively to the behavior of the almost free conduction electrons lying close to the Fermi level, allowing large ring currents to flow within the basal plane. Quantitatively, however, the exact source of this large diamagnetism has eluded investigators for many years. It turns out that the Landau-Peierls formulation is inadequate to explain it, since in graphite there are degenerate bands near the Fermi level and band-to-band transitions must be taken into account. Only recently has a direct calculation of the energy level spectrum been carried out for the general three-dimensional case.[13] This method gives the correct value for the $\chi_{\parallel}$ component, due primarily to conduction carriers. Progressing away from the hexagonal axis, this component would then be expected to drop off rapidly since the electrical conductivity itself is also highly anisotropic[14] $(\sigma_{\perp}/\sigma_{\parallel} \cong 140)$. This component thus decreases effectively to zero, allowing the small ionic core or inner she... 1S electron component to become visible.

4.1. Susceptibility Trace and Anisotropy

The susceptibility trace is defined by

$$\chi_T = \chi_1 + \chi_2 + \chi_3 .$$

In fact, any orthogonal set of measurements, χ_x, χ_y, χ_z, taken on a crystal will still give the same total trace; i.e., χ_T is <u>invariant</u> to a rotation of axes so that

$$\chi_T = \chi_x + \chi_y + \chi_z. \tag{8}$$

For the case of graphite, the ionic core component, χ_I, is isotropic so that in the basal plane, $\chi_1 = \chi_2 = \chi_I = \chi_{\perp}$. The component $\chi_{\parallel}$ is the sum of χ_I plus the conduction carrier component, χ_c. The trace then becomes

$$\chi_T = \chi_{\parallel} + 2\chi_{\perp} = \chi_c + 3\chi_I. \tag{9}$$

However, one does not encounter an "ideal" single crystal since there are usually other small contributions, some of which are additive $(\Delta\chi_{T_1})$ and

---

*Since all susceptibilities discussed in this paper are diamagnetic (except where otherwise stated), any reference to magnitude will mean the absolute value.

16

others which are substractive $(\Delta\chi_{T_2})$. The complete relation for the susceptibility in real graphite is

$$\chi_{T'} = \chi_c + 3\chi_I + \Delta\chi_{T_1} - \Delta\chi_{T_2}, \qquad (10)$$

where

$$\Delta\chi_{T_1} = \Delta\chi_T(R) + \Delta\chi_T(T), \quad \text{and}$$

$$\Delta\chi_{T_2} = \Delta\chi_T(NGC) + \Delta\chi_T(M) + \Delta\chi_T(I).$$

These symbols are defined in the following discussion.

The first of the additive terms, $\Delta\chi_T(R)$, is due to that part of the crystal having the rhombohedral crystallographic modification[15] (abcabc stacking scheme), usually caused by cold working. Pacault et al.[16] observed that certain types of grinding (but not all) caused an initial increase of as much as 12 per cent in the susceptibility of natural graphite flake. This condition occurred within the first two minutes of grinding, going to maximum susceptibility and then decreasing throughout the remainder of the grinding time (as long as four hours). This maximum may be related to the fact that there is also a maximum percentage ($\sim$ 20 per cent[17]) of a crystal that can be converted to the rhombohedral modification by this means. A theoretical model suggests[18] that above 150°K both the rhombohedral and the two-dimensional structures lead to the same trace value of -39×10^{-6} emu/gm. Thus, it would be expected that the maximum contribution from $\Delta\chi_T(R)$ would be -7.8×10^{-6} emu/gm, giving a maximum trace of -26×10^{-6} emu/gm.

The $\Delta\chi_T(T)$ term is due to a turbostratic structure having a random rotation of planes. This structure is considered to be intermediate between the normal three-dimensional and the two-dimensional structures. The high susceptibility value for the turbostratic case has been verified here for pyrolytic graphite (see Section 5) where χ_T and c_o simultaneously decrease with increasing annealing temperature from high initial values becoming asymptotic to their respective single-crystal values.

Of the subtractive terms, $\Delta\chi_T(NGC)$ is caused by any part of the sample that is composed of non-graphitic or amorphous carbon. This contribution has a small susceptibility magnitude, as has been amply demonstrated from studies of the susceptibility behavior of pre-graphitic carbons after heat treatment. The results of Honda[19] are shown in Figure 8a, where the average isotropic $\chi = \chi_T/3$ rises sharply from a value $\sim -0.7 \times 10^{-6}$ emu/gm for a heat treatment at 1400°C to $\sim -6.7 \times 10^{-6}$ emu/gm at 2300°C. Thereafter, it begins to saturate in the final crystallization process reaching a value of -7.5×10^{-6} emu/gm at 3000°C.

The $\Delta\chi_T(M)$ term represents the contribution of those microcrystallites $\lesssim 150$ Å in diameter, where it has been shown [19, 20] (see Figure 8b) for several types of carbon that χ rises with crystallite diameter (assumed

17
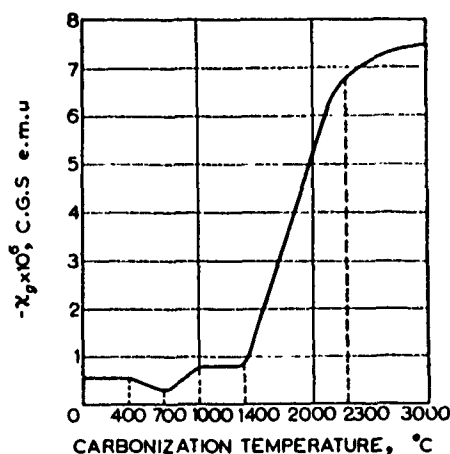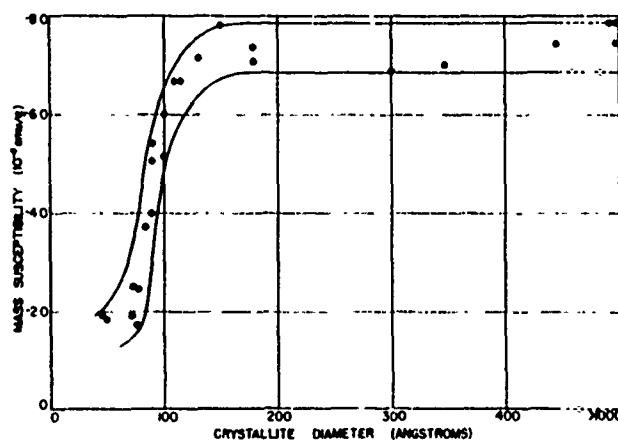
a. (after Honda[19])   b. (after Pinnick[20])   N-4409

Figure 8. Susceptibility of Pre-graphitic Carbon Versus Heat
Treatment Temperature and Resultant Particle Size.

identical to L_a) from $\sim 1 \times 10^{-6}$ emu/gm at ~ 50 Å to $\sim -7.4 \times 10^{-6}$ emu/gm
at ~ 150 Å . It remains constant thereafter out to > 1000 Å. This contribution
is actually an extension of $\Delta\chi_T$(NGC) where the graphite structure is just
beginning to form within each crystallite, but the crystallite's small size
inhibits its effect on the measured susceptibility.

The impurity contribution, represented by $\Delta\chi_T$(I), may be divided
into three categories:

(a) Ferromagnetic agglomerates that can contribute a sizable error.
In Section 1, this contribution was discussed along with the Honda-Owen
method used for its correction.

(b) Non-ionized inclusions of paramagnetic or diamagnetic impurities.
The average susceptibility of paramagnetic elements is $\sim +0.9 \times 10^{-6}$ emu/gm,
excluding a few rarer elements that have very high values. The average
susceptibility for diamagnetic elements is $\sim -0.4 \times 10^{-6}$ emu/gm.   Thus, the
error due to this component for the impurities usually encountered and for
their usual concentration ($\lesssim 10$ ppm), would be 0.0001 per cent.

(c) Ionized impurities, especially if located in substitutional lattice
sites, that can have an effect on the Fermi energy of the conduction electrons
of the host graphite lattice. Thus, such impurities affect χ_c directly and can
make a sizable change. A study of the effect of boron is discussed in
Section 6.

18

4.1.1. Single Crystals

Measurements were made on nine single crystals: six natural ones from Essex Country, New York, purified in chlorine at 3000°C, and three synthetic ones, grown from a super-saturated iron solution at 3200°C[21] and purified. The resulting values are shown in Table 3 for T = 299 ± 1°K along with their respective masses and anisotropies (see Table 1 for typical data).

Table 3. Principal Susceptibilities of Graphite Single Crystals.
(Units of 10^{-6} emu/gm)

Crystal	Mass (mg)	$-\chi_\perp^*(\parallel a)$	$-\chi_\perp^*(\perp a)$	$-\Delta\chi_\perp^*$	$-\chi_\perp$	$-\chi_\parallel$	$\chi_\parallel/\chi_\perp$	$-\chi_T$
EP-53	1.18	0.44 ± 0.02	0.37 ± 0.02	+0.07	0.30 ± 0.02	21.75 ± 0.10	72	22.58 ± 0.15
EP-54	2.33	0.62 ± 0.01	0.47 ± 0.01	+0.15	---	21.35 ± 0.10	45*	22.44 ± 0.12
EP-55	1.32	0.54 ± 0.02	0.55 ± 0.01	-0.01	---	22.04 ± 0.05	41*	23.13 ± 0.08
EP-56	1.55	0.36 ± 0.04	0.33 ± 0.02	+0.03	0.28 ± 0.04	21.35 ± 0.10	76	22.05 ± 0.16
EP-57	0.499	0.63 ± 0.04	0.41 ± 0.02	+0.22	0.34 ± 0.04	21.92 ± 0.04	64	22.98 ± 0.12
EP-58	0.656	0.36 ± 0.01	0.33 ± 0.01	+0.03	0.33 ± 0.01	22.21 ± 0.10	69	22.89 ± 0.12
SP-18	0.318	0.64 ± 0.10	0.53 ± 0.08	+0.11	---	21.48 ± 0.30	41*	22.64 ± 0.48
SP-19	2.18	0.41 ± 0.01‡	0.51 ± 0.01‡	---	---	21.93 ± 0.20	54*	22.84 ± 0.22
SP-20	0.204	0.38 ± 0.05	0.37 ± 0.04	+0.01	0.37 ± 0.04	22.08 ± 0.50	60	22.87 ± 0.60
Weighted mean =		0.49 ± 0.11	0.42 ± 0.08		0.32 ± 0.02	21.83 ± 0.27		22.76 ± 0.25

‡ a-axis orientation unknown.   Optimum value $\chi_\parallel/\chi_\perp$ = 21.83/0.32 = 68.

* calculated from lowest measured $\chi_\perp^*$.

Let us first consider the entire set of measured $\chi_\perp^*$ values where the weighted mean with mean deviation is

$$\chi_\perp^* \text{ (weighted mean)} = -(0.45 \pm 0.09) \times 10^{-6} \text{ emu/gm.}$$

The overall range of values is large and well outside experimental error, since the individually quoted error limits average only ±0.03. In fact, the range is virtually the same as that found by Poquet et al.[22] on crystals of the same origin. In units of 10^{-6} emu/gm, these are

$$-0.33 \text{ to } -0.64 \quad \text{present results}$$
$$-0.33 \text{ to } -0.61 \quad \text{Poquet et al.}$$

This spread of values is believed to be due to the contribution of small secondary parts of a crystal that are misoriented. These misoriented parts can take several forms:

(a)   Twin or simple bend rendering the crystal a bicrystal. Taking the simplest case having a bend down the middle of the crystal of θ degrees up from the basal plane, then from equation (15) on p. 27, $\theta = 7.4°$. None of these crystals could possibly have such a large bend.

(b)   Small crystallite inclusions. If we assume that the crystallites are oriented at random, then 0.83 per cent of the crystal's mass would be involved. This source appears likely as a partial contribution in some of the poorer crystals and would increase the average of the measured values.

(c)   Double-twins of the $(11\bar{2}1)$ type[23] producing narrow planes oriented 20.8° from the (0001) basal plane and perpendicular to an a-axis as shown in Figure 9a. These planes appear as striations on the basal plane surface as shown in Figure 9b. A sufficient number of these can contribute

VIEW IN $[01\bar{1}0]$ DIRECTION

a.   b.
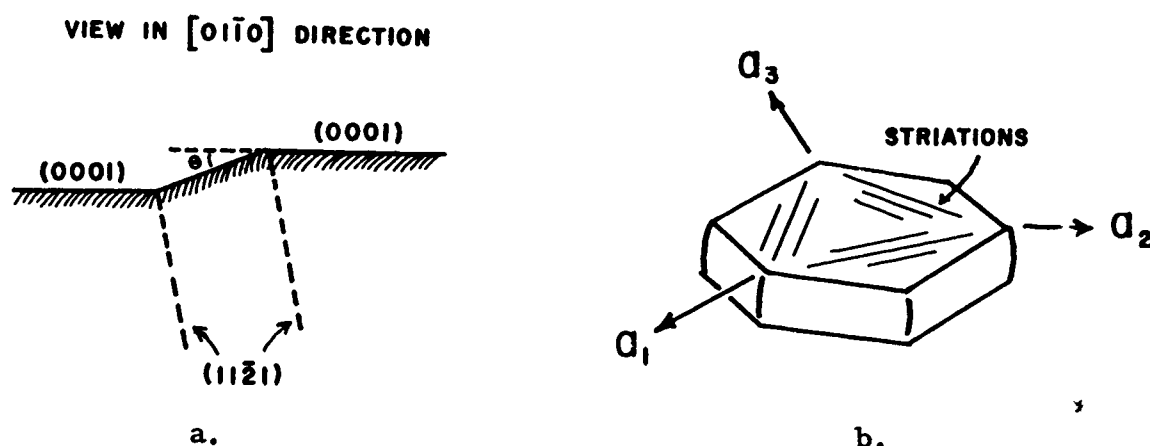
N-4410

Figure 9.   Double-twins in Graphite of the $(11\bar{2}1)$ Type.

to the measured basal plane susceptibility depending on the azimuthal angle ϕ between $\underline{H}$ and a striation. Since macroscopic symmetry arguments[24] state that the susceptibility (a second rank tensor) for a hexagonal crystal structure should have exact isotropy in the basal plane, any azimuthal anisotropy might be due to this twin-plane contribution.

The results of $\chi_\perp^*$ measurements made parallel to the a-axis, $\chi_\perp^*$ (∥ a), and perpendicular, $\chi_\perp^*$ (⊥ a), strongly suggest that there may be a real difference. The weighted means for the two orientations (excluding SP-19 where the a-axis orientation is unknown) in units of 10^{-6} emu/gm are

$$\chi_\perp^* \,(\text{∥ a}) = -0.49 \pm 0.11$$
$$\chi_\perp^* \,(\text{⊥ a}) = -0.42 \pm 0.08.$$

The reality of this difference can best be considered by looking at the individual crystal differences, $\chi_\perp^*$ (∥ a) $-$ $\chi_\perp^*$ (⊥ a) $= \Delta\chi_\perp^*$. These differences, shown in Table 3, indicate that all except one of the crystals shows a positive difference, in accord with that expected from the observed twin-plane contribution. Figure 10 shows pictures of four of the best crystals, SP-20, EP-58, EP-53, and EP-57. These crystals are compared because they are small,

20
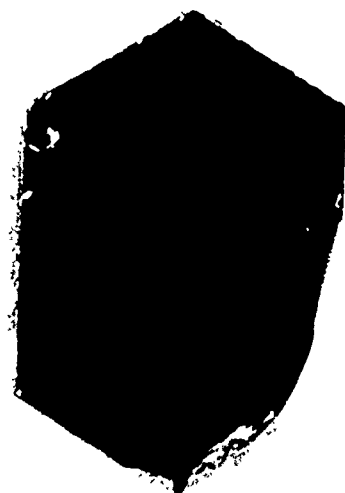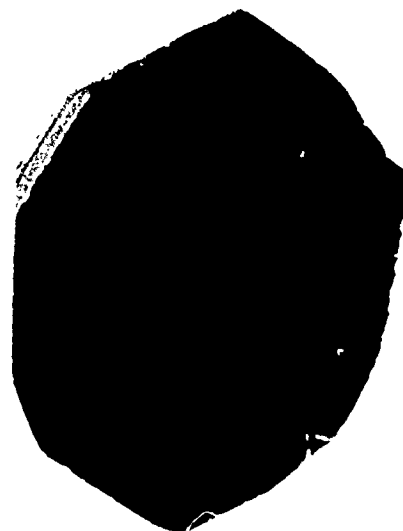
(N-4014)	SP-20	(N-4013)	EP-58
(N-4007)	EP-53	(N-4011)	EP-57
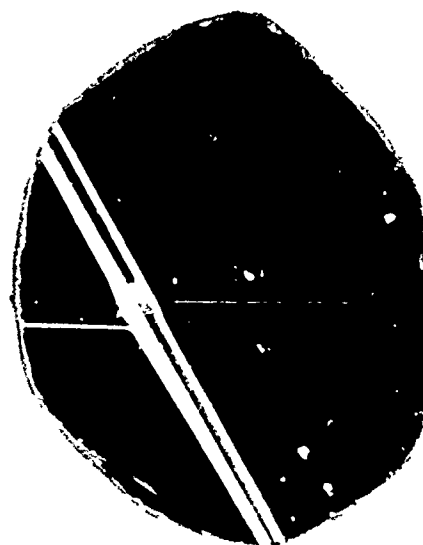
Figure 10. Photomacrographs of Four of the Best Crystals
Showing the Degree of Twinning.

about the same size, and reasonably regular in shape. They have been placed in order of perfection, that is, in ascending degree of twinning. Comparison of their $\Delta\chi_{\perp}^{*}$ values shows a direct correspondence. SP-20 and EP-58, the two best crystals, show very little twinning (SP-20 none and EP-58 one) and have correspondingly low $\chi_{\perp}^{*}$ and $\Delta\chi_{\perp}^{*}$ values. Though this trend also can be seen for the rest of the crystals, there are additional complications, such as the presence of small deformed portions (type b) or large and/or irregular crystal shapes. Where contributions of type b can be considered negligible, for the azimuthal angle ϕ, the true basal plane susceptibility, $\chi_{\perp}$, is related to the measured value $\chi_{\perp}^{*}$ (see equation 15) by

$$\chi_{\perp}^{*} = \chi_{\perp} + A(\chi_{\parallel} - \chi_{\perp}) \sum_{i=1}^{3} N_i m_i \sin^2 \left[\text{arc tan} (\sin \phi_i \tan \theta) \right] \quad (11)$$

where $\theta = 20.8°$, $N_i =$ number of striations of the ith orientations, $m_i =$ mass fraction per i^{th} striation, and A is an empirical constant to be determined. A count of the N's and m's giving a weighting to the area of the individual striations was made using individual sample photographs. Using a value of $\chi_{\parallel} - \chi_{\perp} = -21.5 \times 10^{-6}$ emu/gm, the value of A could then be determined from the difference in the two measured orientations, $\Delta\chi_{\perp}^{*}$. The resultant individual crystal $\chi_{\perp}$ values calculated for five of the best crystals are shown in Table 3. As indicated, the best value for $\chi_{\perp}$ is found to be

$$\chi_{\perp} = -(0.32 \pm 0.02) \times 10^{-6} \text{ emu/gm.}$$

It is interesting that this component represents the ultimate term in a series of polynuclear aromatic ring systems[25, 22] starting with benzene (-0.44×10^{-6} emu/gm), to naphthalene (-0.43×10^{-6} emu/gm), to anthracene (-0.39×10^{-6} emu/gm), on to graphite with its effectively infinite ring system. Also from another point of view, we would expect this value to be close to that of diamond (-0.49×10^{-6} emu/gm), an insulator in the pure state having no conduction carrier component.

Turning our attention to the maximum susceptibility component, the weighted mean value of $\chi_{\parallel}$ is

$$\chi_{\parallel} \text{ (aver.)} = -(21.83 \pm 0.27) \times 10^{-6} \text{ emu/gm,}$$

where the error quoted is the mean deviation of the measured values on the individual crystals. The weighted mean of the trace value is

$$\chi_{T} \text{ (aver.)} = -(22.76 \pm 0.25) \times 10^{-6} \text{ emu/gm.}$$

The individual anisotropy ratios, $\chi_{\parallel}/\chi_{\perp}$, vary widely from 41 to 76. However, with the $\chi_{\perp}$ value quoted above, we can predict an ultimate value for an ideal crystal of

$$\chi_{\parallel}/\chi_{\perp} = 21.83/0.32 = 68.$$

The crystal EP-58 is the closest approximation to this ideal crystal.

22

It is of interest to compare these results with previous susceptibility values. Because of graphite's large anisotropy, most anisotropy measurements have been made by the Krishnan torque method, [26] which consists of finding the torque or period of oscillation of the crystal in a homogeneous magnetic field giving the difference $\chi_\| - \chi_\perp$. To find the separate values, an independent measurement of $\chi_\perp$ was usually carried out by the Rabi null method[27] that involved detecting the movement of a crystal immersed in a liquid (KI solution) whose susceptibility could be varied through that of the crystal. The contribution of the present study has been to measure the complete orientation dependence <u>directly</u> by the Faraday method, using very sensitive techniques on highly purified, quite perfect single crystals. These values, normalized to 299°K, are summarized chronologically in Table 4.

Table 4. Diamagnetic Susceptibility of Graphite Single Crystals at 299°K
(Units of 10^{-6} emu/gm)

Authors	$-\chi_\|$	$-\chi_\perp$	$-\chi_T$	$\chi_\|/\chi_\perp$	Sample	Method
Honda and Sone'(1913)[28]	14.0, 6.1	2.2	22.3	6.4	4 Ceylon crystals	Faraday
Guha and Roy (1934)[25]	22.4	0.37	23.1	60	11 Ceylon crystals	Torque (Rabi)⁺
Krishnan and Ganguli (1939)[30]	21.5	0.5	22.5	43	3 Ceylon crystals	Torque (Faraday)
Donoghue and McClelland (1951)[31]	12.5, 5.4	5.3	23.3	--	Pressed Ceylon flake pellet	Faraday
Poquet et al. (1960)[22]	20.9	0.33*	21.6	63	4 Essex County crystals, purified	Torque (Faraday, Rabi)⁺
Present work	21.8	0.32	22.8	68	6 Essex Country crystals, purified; 3 Synthetic, purified	Faraday

*Minimum value observed.
⁺$\chi_\perp$ measured by method in parentheses.

The early measurements of Honda and Sone', [28] though made by the Faraday method, used crude impure Ceylon natural crystals. Their trace values ranged from -12.5×10^{-6} emu/gm to -22.3×10^{-6} emu/gm, the best value given in the table. An overall average of the 11 crystals measured by Guha and Roy[29] is given for χ_T, though the authors themselves threw out their two lowest values. It is interesting that their crystals ranged in mass from 32-100 mg, whereas ours, seen in Table 3, ran from 0.20-2.3 mg, a factor of 40 smaller. This comparison gives an indication of the relative forces involved and the difficulty of measuring $\chi_\perp$, for instance. The results of Krishnan and Ganguli, [30] made in the same laboratory used by Guha and Roy, with presumably the same type of Ceylon single crystals, obtained a good trace value, although their $\chi_\perp$ value was a rough determination by the Faraday method, using the inhomogeneous part of their standard flat-pole piece magnet. The measurements of Poquet et al.[22] were made on crystals prepared in this laboratory. Their starred $\chi_\perp$ value is the minimum value observed, although a range of values was actually observed as discussed on page 19. Guha and Roy's $\chi_\perp$ value, measured on two of their crystals, also comes close to this value. The results quoted by Donoghue and McClelland[31] are instructive; but since their sample consisted of a pressed pellet of Ceylon flake, a certain percentage of

rhombohedral modification might have raised its trace value somewhat. Our trace value comes quite close to the overall average value of -22.6×10^{-6} emu/gm.

4.1.2. Polycrystals

The application of the above results on single crystals rests on the fact that the susceptibility trace is <u>invariant</u> to a transition from the single to ideal polycrystalline form.[32]   Here an "ideal" polycrystal is defined as a matrix of perfect crystallites having no intercrystalline matter where $\Delta\chi_{T_1} = \Delta\chi_{T_2} = 0$. This invariance is a direct consequence of equation (8), since one can make a direct transformation crystallite by crystallite. For an actual poly-crystalline graphite, however, we have two additional considerations:

a.   There is a degree of preferred orientation in the measured anisotropy.

b.   The intercrystalline material, principally binder, generally con-tains a certain amount of non-graphitic carbon, leading to a larger value of $\Delta\chi_{T_2}$.

These differences, as seen in the susceptibility measurements once one can rely on the single crystal values, enable us to obtain valuable additional in-formation about the various types of real graphite.

Measurements have been carried out on several graphites varying in starting material, method of fabrication, subsequent heat treatment (see Section 5) and doping with boron (see Section 6). Table 5 lists these results,

Table 5. Principal Susceptibilities of Different Graphites
(Units of 10^{-6} emu/gm)

Sample	Fabrication	Density (gm/cc)	$-\chi_1$	$-\chi_2$	$-\chi_3$	$-\chi_T$	χ_{max}/χ_{min}
Single Crystal	---	2.26	22.1*	0.32	0.32	22.8	68
Pyrolytic - Diefendorf (3600°C) sample	pyrolysis	--	19.1*	0.75	1.08	20.9	25
Pyrolytic - PF-27, B-1 (3000°C)	pyrolysis	2.22	19.2*	0.88	0.98	21.0	22
Pyrolytic - PF-8 (3360°C)	pyrolysis	2.26	17.8*	1.06	1.48	20.3	17
ZT-1	} molded	2.01	9.54*	4.43	5.10	19.1	2.15
ZT-2			9.44*	4.52	5.15	19.1	2.09
AGK-SP-1 (7ppm boron)	} extruded	1.64	4.16*	7.95	7.73	19.8	1.91
AGK-SP-2			4.27*	8.35	8.20	20.8	1.96
ATJ	molded	1.68	8.08*	6.01	6.20	20.3	1.34
L 113-SP	extruded	--	6.95*	7.08	7.06	21.1	1.02
CEP	molded	1.61	7.09*	7.03	7.02	21.1	1.01

*Component parallel to c-axis, across the grain, in extrusion direction or in molding direction; whichever applies.

showing anisotropies ranging from the almost isotropic lampblack-based grade CEP with a value of 1.01 to a single crystal with a value of 68. Table 5 shows the following characteristic behavior: for extruded samples, one low component along the extrusion direction and two high ones perpendicular to this direction; and for the molded samples, one high component along the molding direction, with two low ones for the other two orientations. This behavior comes about for the extrusion process because the crystallites, which are somewhat elongated along the basal plane, align preferentially along the extrusion direction. On the other hand, in the molding process, these particles are compressed with their long axes preferentially perpendicular to the molding direction. An interesting example of this behavior is seen by comparing grades CEP and L113-SP which both have a lampblack base, having similar particle and binder processing except for the method of fabrication: grade CEP is molded and grade L113-SP is extruded. Although they have identical trace values, -21.1×10^{-6} emu/gm, the distribution of the principal susceptibility components reflects their respective fabrication processes.

The trace values reflect the relative values of $\Delta\chi_{T_1}$ and $\Delta\chi_{T_2}$. For example, the coke-base graphites, ZTA, AGK-SP, and ATJ, have lower trace values than the lampblack base CEP and L113-SP. The main difference is governed by $\Delta\chi_{T_1}$, where X-ray measurements show that the latter types have a high degree of turbostraticity. $\Delta\chi_{T_2}$ serves to lower the entire set of values below that of a single crystal. As an example, the final values for pyrolytic graphites heated to 3360°C average $\sim -21 \times 10^{-6}$ emu/gm, effectively that of a single crystal minus a small increment $\Delta\chi_{T_2}$.

As a demonstration of the method of obtaining these numbers, of the anisotropies encountered, and of the absence of ferromagnetic impurities, Figure 11 shows Honda-Owen plots for pyrolytic PF-27, and grades AGK-SP, ATJ, and CEP.

4.2. Susceptibility Orientation Dependence

4.2.1. Single Crystals

The orientation dependence for an ideal crystal may be determined by again considering equation (3). If we choose a primed system of coordinates such that $\underline{H}$ is parallel to the x'-direction, then $H'_y = H'_z = 0$; and equation (3) becomes

$$\Delta E_s = \frac{\mu_c}{2} \rho \int \chi_H H^2 dv . \tag{12}$$

On the other hand, if we choose the principal magnetic axes, we have equation (4). But, the potential energy represented here must be independent of any choice of axes, so that

$$\chi_1 H_x^2 + \chi_2 H_y^2 + \chi_3 H_z^2 = \chi_H H^2 . \tag{13}$$

25
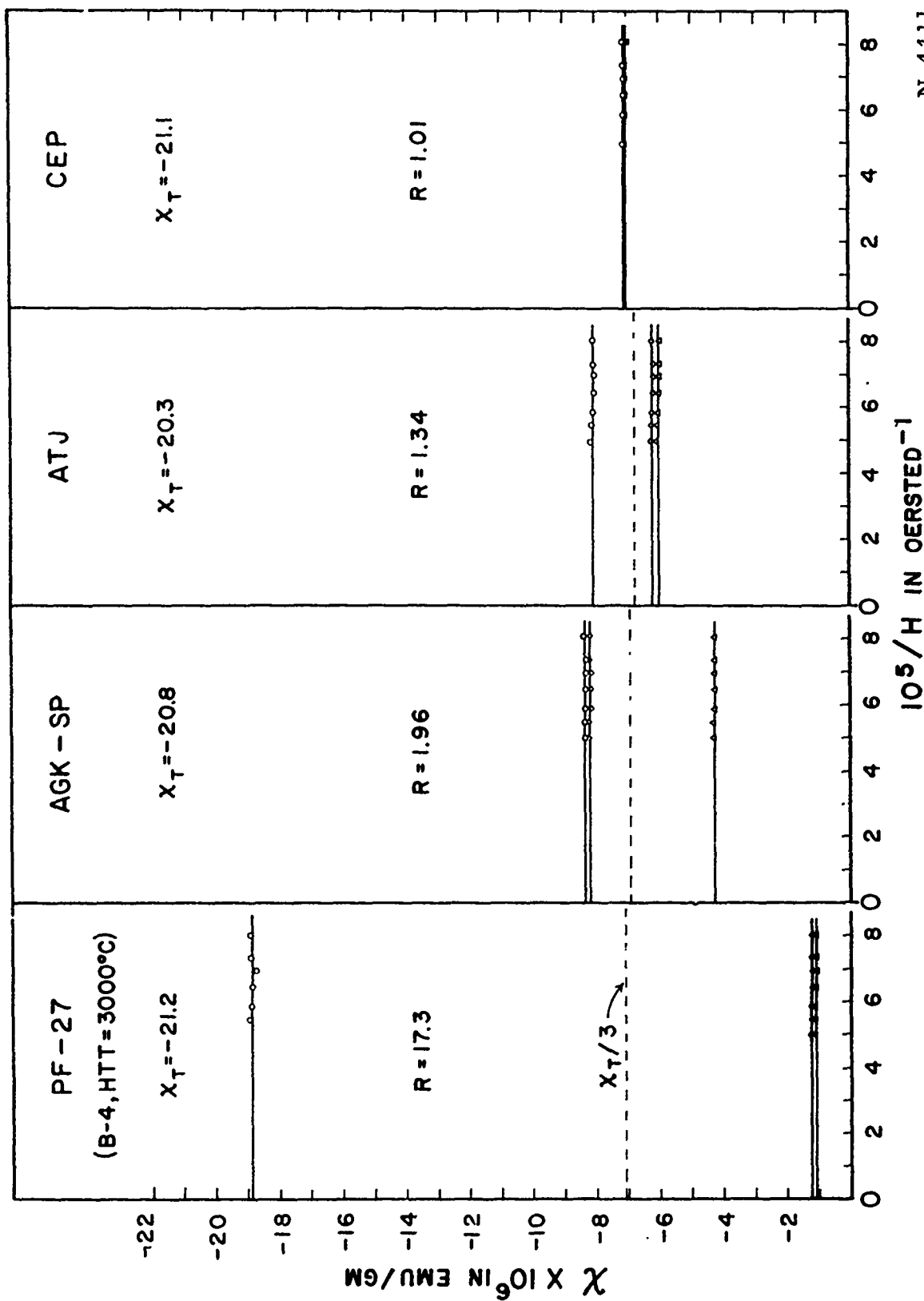
Figure 11. Honda-Owen Plots for Pyrolytic Graphite PF-27 and Grades AGK.-SP, ATJ, and CEP.

N-4411

And if $\underline{H}$ makes angles with these axes having direction cosines l, m, and n, then

$$\chi_1 l^2 + \chi_2 m^2 + \chi_3 n^2 = \chi_H \; . \tag{14}$$

For graphite, introducing $\chi_{\parallel}$ and $\chi_{\perp}$ as defined above, this relation becomes

$$\chi_H = \chi_{\perp} + (\chi_{\parallel} - \chi_{\perp}) \cos^2 \theta, \tag{15}$$

where θ is the angle between $\underline{H}$ and the c-axis. Although this relation has been implicitly assumed in previous measurements on graphite, it had not been proven by a direct measurement. Herein lays the power of the Faraday method. A typical curve for EP-54 is shown in Figure 12, where the solid curve is given by equation (15) with the parameters in units of 10^{-6} emu/gm giving

$$\chi_H = -0.47 - 20.88 \cos^2\theta \; .$$

This fit is excellent, exhibiting a deviation well within experimental error. EP-53 and SP-18 also were found to obey equation (15) exactly. This investigation represents the first direct experimental proof of the cosine-squared behavior in graphite single crystals.

4.2.2. Polycrystals

Although this cosine-squared relation holds well for single crystals, it is not immediately obvious that it should also hold even for an ideal polycrystal. In fact, it was originally thought that some information might be obtained from a deviation from such a behavior. It can be shown,[33] however, that when there is preferred orientation of the crystallites—that is, along the extrusion or molding directions—a cosine-square behavior is also obeyed for a real polycrystal. Figure 13 shows the experimental results of orientation measurements taken on ZTA and pyrolytic graphite cubes. The curves give the theoretical cosine-squared behavior, again demonstrating an excellent fit. Grade AGK-SP was measured also, but it is so similar to grade ZTA that it could not be resolved on this figure. The observed principal values for grades ATJ and CEP with their corresponding computed cosine-squared curves are shown to demonstrate the progression in the range of anisotropies.

These anisotropies are, of course, related to the degree of preferred orientation of crystallites. One would expect to see a correlation between the anisotropy determined from these susceptibility values and that obtained from X-ray studies. Spence[33] has made a comparison for the case of AGK-SP and finds a reasonable agreement.

27
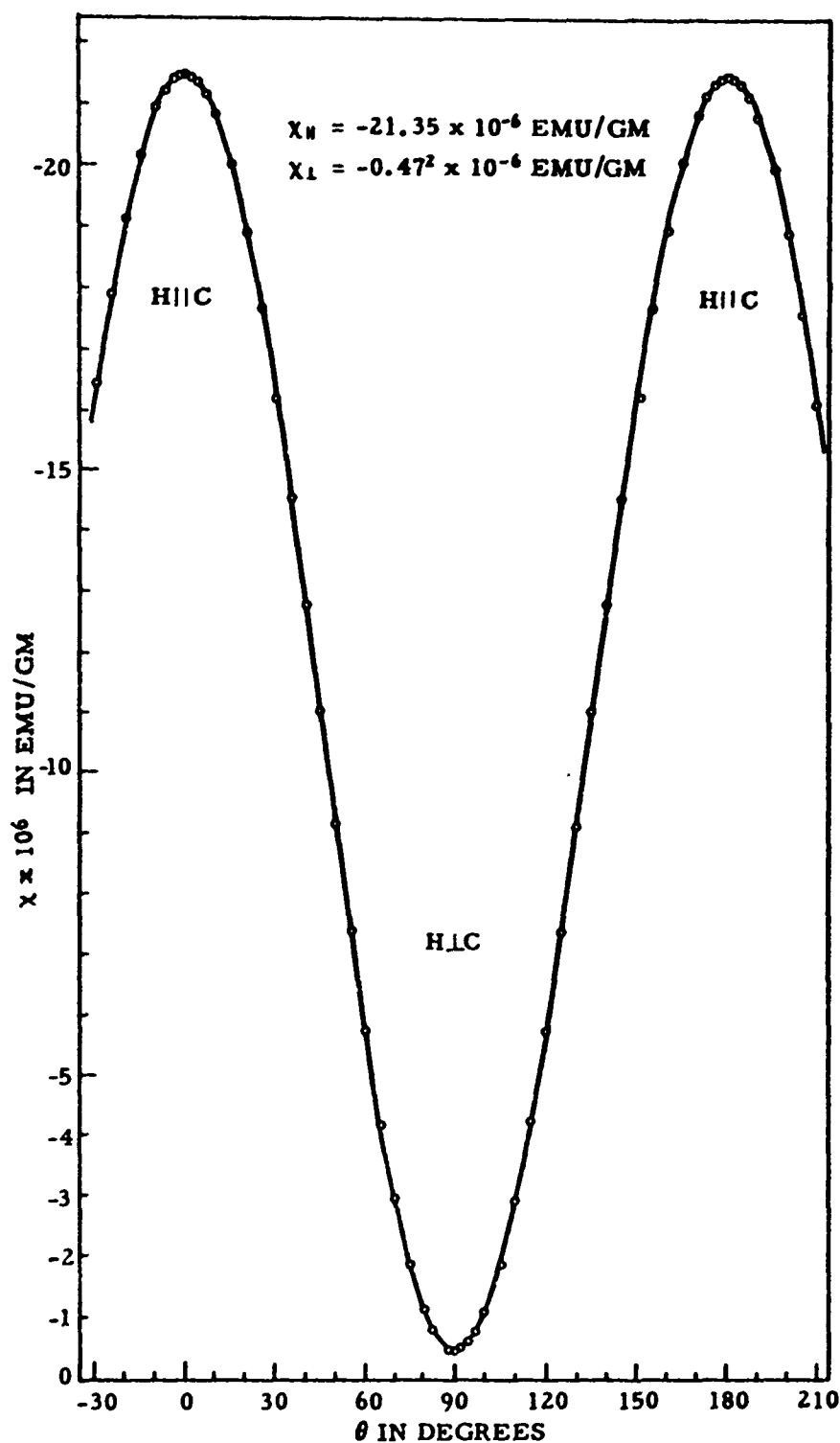
N-4412

Figure 12. Orientation Curve for the Single Crystal EP-54;
Solid Line Is Cosine-Squared Curve.

28
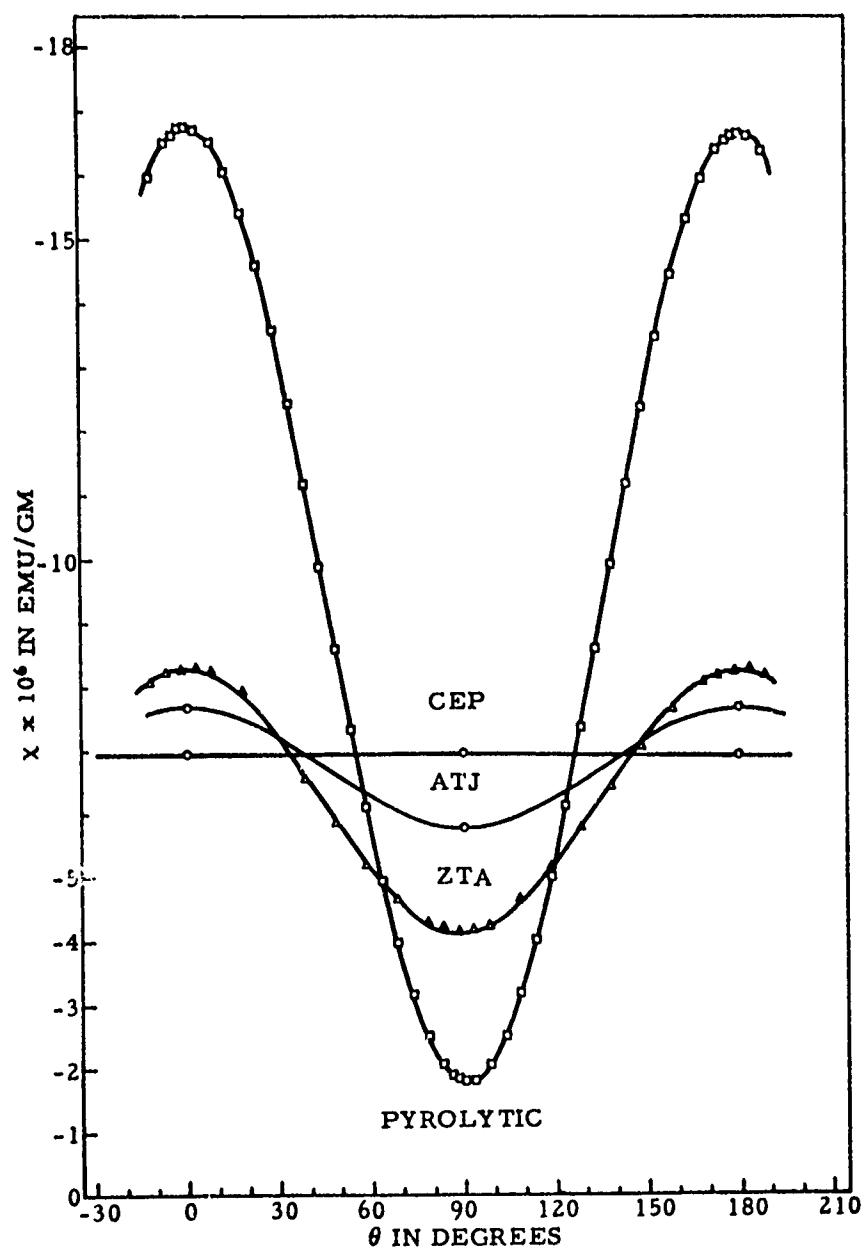
Figure 13. Orientation Curves for the Graphite Polycrys.als: Pyrolytic, Grades ATJ, ZTA, and CEP; Solid Lines Are Cosine-Squared Curves.

5. SUSCEPTIBILITY DEPENDENCE ON ANNEALING TEMPERATURE OF PYROLYTIC GRAPHITE

5.1. Sample Characterization and Heat Treatment

A study was made on the effect of annealing temperature, in the range 2000°C to 3360°C, upon the susceptibility anisotropy and trace of three types of pyrolytic graphite. These included one sample (PA-3) made by M. B. Manofsky at the Fostoria Development Laboratory of National Carbon Company and two (PF-8 and PF-27) made by R. L. Finicle at this laboratory. Critical pyrolysis conditions as well as pertinent properties[34] of the resulting pyrolytic graphites are summarized in Table 6. The impurity content was

Table 6. Growth Conditions for Pyrolytic Graphites

Type	Substrate	Deposition Temperature (°C)	Gas Composition	Pressure (mm Hg)	Deposition Rate (gm/cm²/sec × 10⁴)	Soot Content	Impurity Content (ppm)	Density (gm/cc)	Resistivity (Microhm-cm)
PA-3 (FE-1710)	Grade CS-312 Slab	2000	4:1:40 CH_4:A:H_2	760	0.0015	possible	≤10	2.24	83.6
PF-8	Grade RT-0008 Strip	2000-2050	1:1.2 CH_4:He	80	1.02	nil	≤10	2.22	402
PF-27	Grade RT-0008 Strip	2100	1:3 CH_4:He	280	1.02	nil		2.22	847

determined by a spectroscopic analysis of a representative sample from Finicle's material. Since the electrical resistivities for Finicle's samples were measured by him on the entire strip, they are to be considered only in a relative sense.

Subsequent annealing treatments in an argon atmosphere were carried out in a tube furnace with a hold time at temperature of one hour. The overall investigation can be divided chronologically into two series:

a. The first measurements, somewhat preliminary in nature, were done with PA-3 and PF-8 using individual samples, each heated to a different temperature.

b. The second set using PF-27, a very good pyrolytic, was carried out in much more detail to characterize the samples and their subsequent treatment in a more systematic way. Sample PF-27 was cut in half and a photomacrograph taken showing the adjacent faces as shown in Figure 14. Side 1 represents the sample as received (2100°C) and side 2 shows the sample after heating to 3360°C. The section marked "x" was chosen as the most uniform region since it was located on the enlarged side of the "dog bone" facing the cooler incoming gas stream, thereby reducing the probability of possible soot inclusions. Figures 15a and 15b are enlarged views of these "x" regions which show clearly in the initially deposited material the tight-knit conical type structure emanating from nucleation

Side 1.
2100°C

Side 2.
3360°C

Figure 14. Photomacrograph of Adjacent Faces of PF-27
Pyrolytic Graphite

N-4426

31
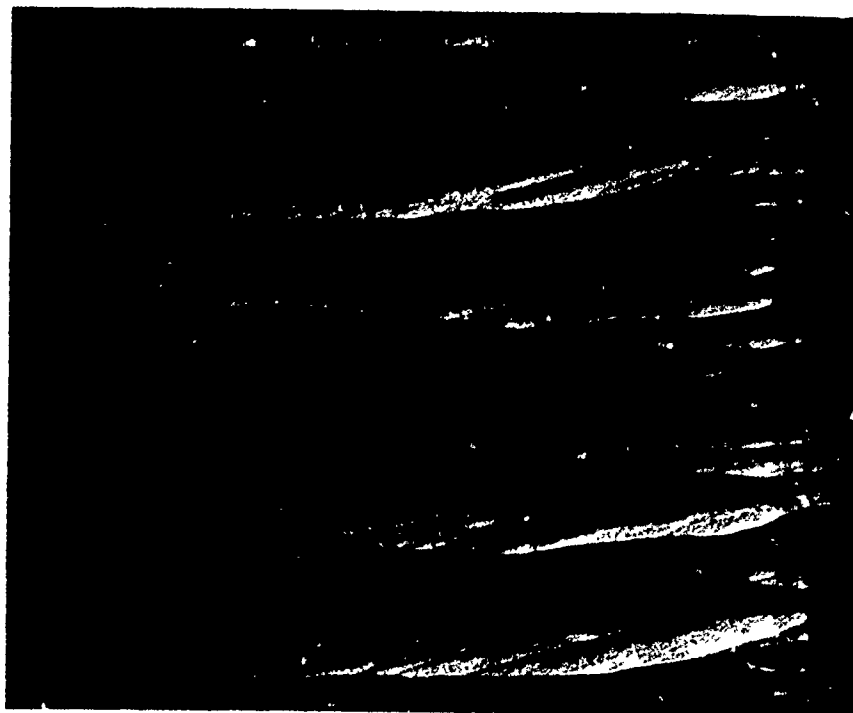
Side 2.
3360°C

N-4428

b.

Side 1.
2100°C

N-4427

a.
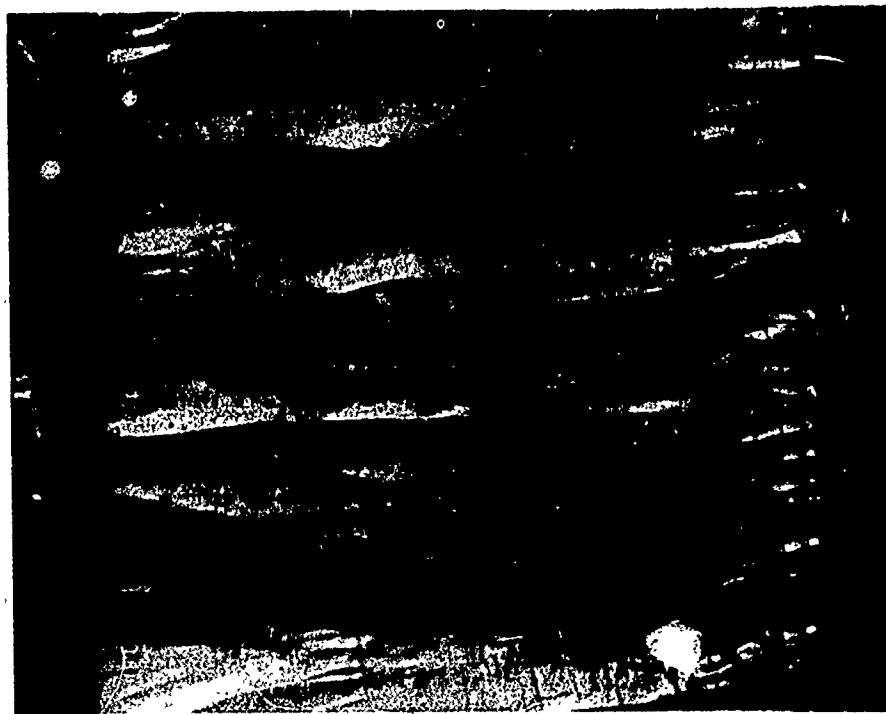
Figure 15.   Photomicrographs of "x" Positions Showing
Effect of Heating to 3360°C.

32

points on the substrate. Rippling in the basal plane structure is outlined by the light bands. The transformation brought about by the high temperature annealing, producing a consolidation into larger more uniform grain structure, is clearly shown in Figure 15b. Figure 16 shows the sample sectioning scheme employed on side 1. The central "B" blocks were used for susceptibility measurements, B-1 and B-4 being measured successively after subsequent heat treatments at 2100°C (as received), 2400°C, 2600°C, 2800°C, 3000°C, 3200°C, and 3360°C. Samples B-2 and B-3, on the other hand, were heated directly to 3360°C and remeasured to ascertain what difference the particular heating-cycle method might have had. Adjoining blocks marked "A" and "C" were reserved for X-ray measurements to determine the variation of the lattice spacings, a_o and c_o, and the crystallite size in the c-direction, L_c.
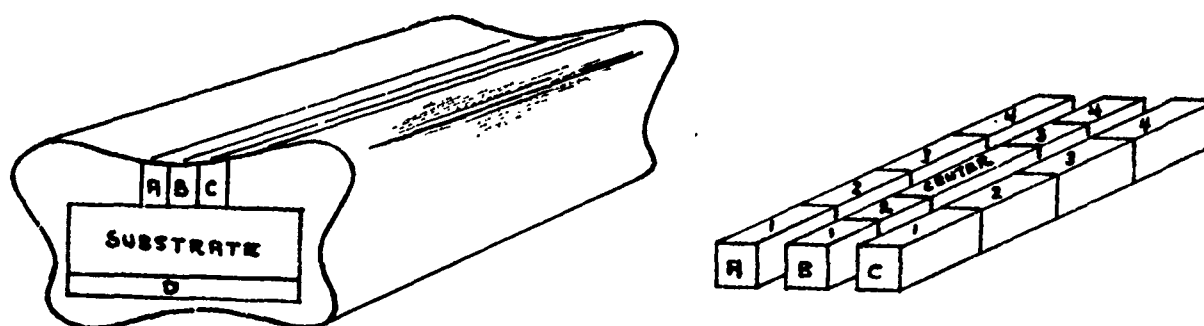
N-4414

Figure 16. Sample Sectioning Scheme Used on PF-27 Pyrolytic Graphite.

5.2. Susceptibility Results

5.2.1. Individual Component and Anisotropy Behavior

The results shown in Figure 17 demonstrate, in general, that with increasing annealing temperature, there is an increase in the absolute magnitude of $\chi_\parallel$ and a decrease in $\chi_\perp$. This behavior is caused primarily by the partial annealing effect in flattening out the layer planes. It is substantiated by direct visual observation (see Figure 15), and by measurements of the electrical resistance made by Finicle.[34] His results on samples cut from PF-8 and PF-27 (designated by him as 8B1 and 27A, respectively) when heated to 2800°C showed the following changes:

	Sample 8B1	Sample 27A
a-direction expansion (direct linear meas.)	3.1%	1.0%
c-direction contraction (direct linear meas.)	4.3%	1.0%
density (gm/cc)	2.225 → 2.262	2.220 → 2.247
electrical resistivity (microhm-cm)	—	430 → 55

33
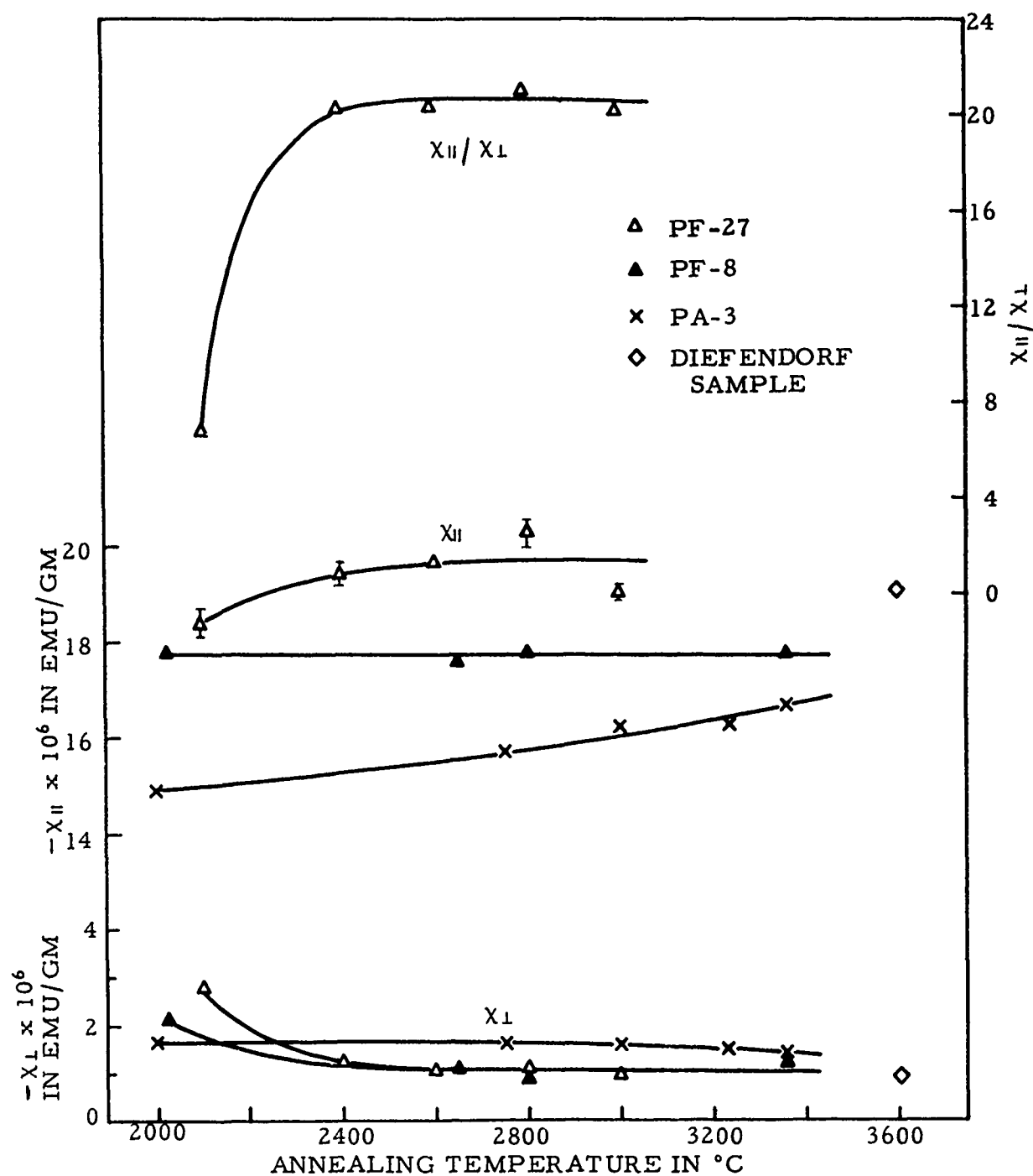
N-4415

Figure 17. Behavior of $\chi_{\parallel}$, $\chi_{\perp}$, and $\chi_{\parallel}/\chi_{\perp}$ for PF-27,
PF-8, and PA-3 Pyrolytic Graphite.

As further evidence of the trend toward lamellar structure, both PF-27 samples showed partial cleavage at $T \gtrsim 3000\,°C$ along the basal plane due to a breakdown of cross-linking during the annealing process. Small cracks of this type also can be seen in the photomicrograph of Figure 15. Since such a slight curling of the planes gives misleading $\chi_\perp$ and $\chi_{\parallel}$ values, these were not plotted beyond $3000\,°C$.

A significant difference between the PA-3 and the PF-8 and PF-27 behaviors is evident, however, in the rate of change with temperature. In the former sample, smooth variations of both $\chi_{\parallel}$ and $\chi_\perp$ caused a gradual increase in the anisotropy. This condition is due to improved alignment of crystallites. The latter samples, on the other hand, showed a rapid increase of $\chi_{\parallel}/\chi_\perp$ in the $2000\,°-2400\,°C$ range, caused primarily by 64 per cent and 43 per cent decreases in $\chi_\perp$, respectively. Thereafter, these values remained constant up to the highest temperature measured. This rapid drop is related to alignment of planes <u>within</u> the crystallites, as will be discussed below in connection with the trace behavior.

5.2.2. Trace Behavior

Behaviors of the susceptibility traces with annealing temperature are shown in Figure 18. These variations reflect the competition between two processes:

a.   an increase due to further graphitization of remaining non-graphitic carbon with an accompanying increase in crystallite size; and

b.   a decrease due to the transformation from a turbostratic to an ordered three-dimensional graphite structure.

In PA-3, the former dominates the trend, where χ_T increases gradually from an initial low value of -18.2×10^{-6} emu/gm up to -19.5×10^{-6} emu/gm.

In the case of PF-8 and PF-27, though process (a) is operative to a certain degree, the dominant behavior is due to process (b). For PF-27, the initial χ_T value of -24.0×10^{-6} emu/gm drops at $T \leq 2400\,°C$ to a steady value of -21.6×10^{-6} emu/gm—effectively that of a single crystal minus a small increment due to non-graphitic material. This trend closely follows the behavior of the interlayer spacing, c_o, which starts from a turbostratic value of 6.82 Å, dropping to the normal value of 6.71 Å at $T \leq 2400\,°C$ and then leveling off. At the same time, a_o remains essentially constant throughout. The behavior of PF-8 is similar except that it starts at a lower χ_T. Figure 17 shows that the decrease in $\chi_\perp$ is dominant in this same initial temperature region; thus while c_o is decreasing, the interlayer interaction is actually also decreasing—presumably due to the elimination of cross-link bonding effects. The fact that L_c grows smoothly throughout the temperature region—a common behavior—shows that beyond about $2600\,°C$, the crystallites are only increasing in size. There is no further appreciable formation of new crystallites $\gtrsim 150$ Å in size. In this discussion, it is assumed that L_c is approximately equal to L_a, the pertinent dimension here. It would, of
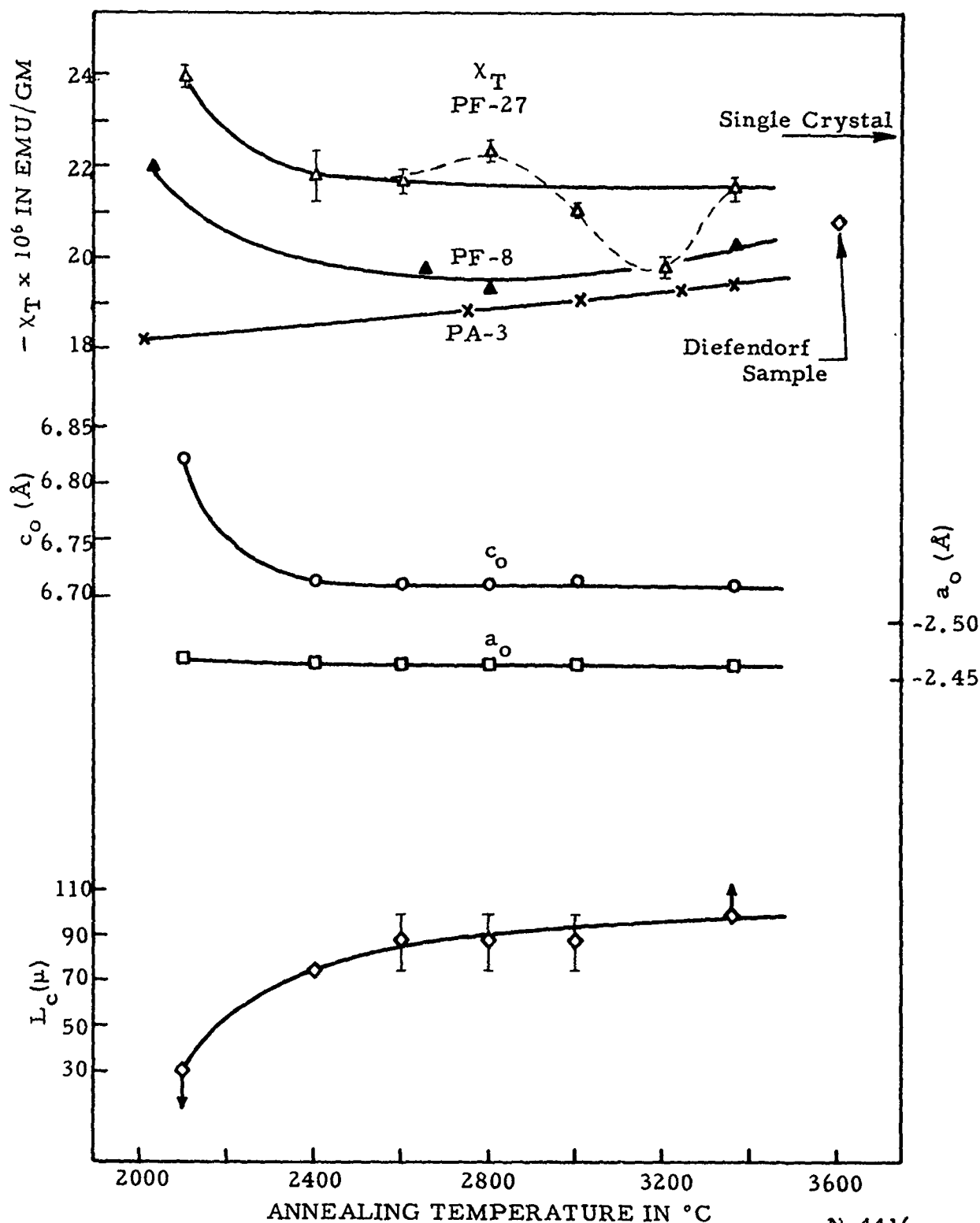
Figure 18. Behavior of the Susceptibility Trace for PF-27, PF-8, and PA-3 Pyrolytic Graphites with Annealing Temperature. For Comparison, L_c, c_o, and a_o Are Shown as Measured on PF-27.

N-4416

36

course, be preferable to know the behavior of L_a directly; however, this information is considerably more difficult to extract from the X-ray results. A rough X-ray search for possible rhombohedral modification showed an erratic behavior, probably due primarily to sample handling and, therefore, is untrustworthy. Observation of the "as received" material, however, showed $\underline{no}$ rhombohedral lines (i.e., ≤ 1 per cent of sample) which may be significant.

Quantitatively, the initial χ_T values show the competition between $\Delta\chi_{T_2}$ and $\Delta\chi_T(T)$. In PA-3, soot inclusions are strongly suspected to be the cause of the low value. Though not seen in this particular sample, they have been observed in material deposited in a similar manner. In addition, there is undoubtedly a certain percentage of microcrystals present. Assuming that $\Delta\chi_T(NGC) = \Delta\chi_T(M) \simeq -3 \times 10^{-6}$ emu/gm and that $\Delta\chi_T(T) = \Delta\chi_T(I) = 0$, then one finds that 17 per cent of the sample's mass is of this type. Though the subject is still rather speculative at present, this value appears rather high. Perhaps impurities also contribute. In fact, the impurities may even be paramagnetic, producing a sizable effect.

In the case of PF-27, where we have the layer spacings, Franklin's relation[35] between the degree of turbostraticity and the d-spacing $(d = c_0/2)$ can be applied. For a completely random rotation of planes, she sets $d_{max} = 3.44$ Å. The probability of finding a random pair is given by

$$P^2 = 1 - \left(\frac{3.44 - d}{3.44 - 3.35}\right) \tag{17}$$

For PF-27, there is 82 per cent turbostraticity. Assuming,

$$\Delta\chi_T(T) = -(24.0 - 21.6) \times 10^{-6} = -2.4 \times 10^{-6} \text{ emu/gm},$$

$$\Delta\chi_T(NGC) + \Delta\chi_T(M) = -(22.8 - 21.6) \times 10^{-6} = -1.2 \times 10^{-6} \text{ emu/gm},$$

and

$\Delta\chi_T(I) = 0$, then the susceptibility trace predicted for complete turbostraticity would be

$$\chi_T(T) = -26 \times 10^{-6} \text{ emu/gm}.$$

At first sight, this value seems reasonable, since it is intermediate between the single-crystal value and that predicted for an ideal two-dimensional model; however, Fischbach[36] has reported an initial value as high as -27.6×10^{-6} emu/gm, and recently Wagoner[37] reports, from measurements made by one of us on his pyrolytic samples with this apparatus, a maximum value as high as -33.5×10^{-6} emu/gm. It appears, then, the assumption that $\Delta\chi_T(NGC) + \Delta\chi_T(M)$ is constant throughout the temperature range is incorrect, and this contribution decreases over this temperature range, as might be implied by the L_c behavior. The relative contribution of each of

these factors in the initial "as received" state is virtually impossible to know with our present information.

In the final state, however, we have more confidence in the situation. By the time the temperature has reached ~ 3200°C, the grain size has fairly well saturated and any amorphous carbon which will crystallize has already done so (see pp. 17, 18). We will find that all of the curves for the better pyrolytics tend toward values which are characteristic of a single crystal[38] minus a certain increment due to the remaining "locked in" non-graphitic carbon. This condition is true not only for PF-8 and PF-27 measured here, but also for a sample of Diefendorf that we measured and for the measurements of Fischbach.[36] These values (in units of 10^{-6} emu/gm) are shown in Table 7 with their accompanying lower limit of annealing temperature and calculated percentages of remaining non-graphitic carbon.

Table 7. Susceptibility of Annealed Pyrolytic Graphite Samples

Sample	Annealing Temp. (°C)	$-\chi_T$ (10^{-6} emu/gm)	Per Cent Non-Graphitic Carbon
PF-8	≥ 3200	20.3	9
PF-27	≥ 3200	21.6	3
Fischbach[36]	≥ 3200	21.0	6
Diefendorf Sample	3600	20.9	8

One final remark about the behavior of the annealing curves can be made. It has been widely believed for some time that both deposition rate and temperature are major factors governing the nature of pyrolytic graphite. The results of Fischbach[36] on pyrolytic graphite deposited in the higher temperature range of 2100°-2300°C revealed a peculiar minimum in χ_T at ~ 2900°C. This minimum seems to vary with deposition temperature, vanishing at ~ 2000°-2100°C, in general agreement with our results. It is possible that the "scatter" of the 2800°C and 3200°C points in Figure 18 may actually be due to this effect producing a minimum at ~ 3200°C. Wagoner[37] has recently extended the investigation of deposition temperatures by studying samples grown at temperatures ranging from 1600° to 2500°C, where a maximum in χ_T of the initial material is seen at $T \simeq 2300°-2400°C$.

6. DEPENDENCE OF SUSCEPTIBILITY AND TRANSPORT PROPERTIES ON BORON CONCENTRATION
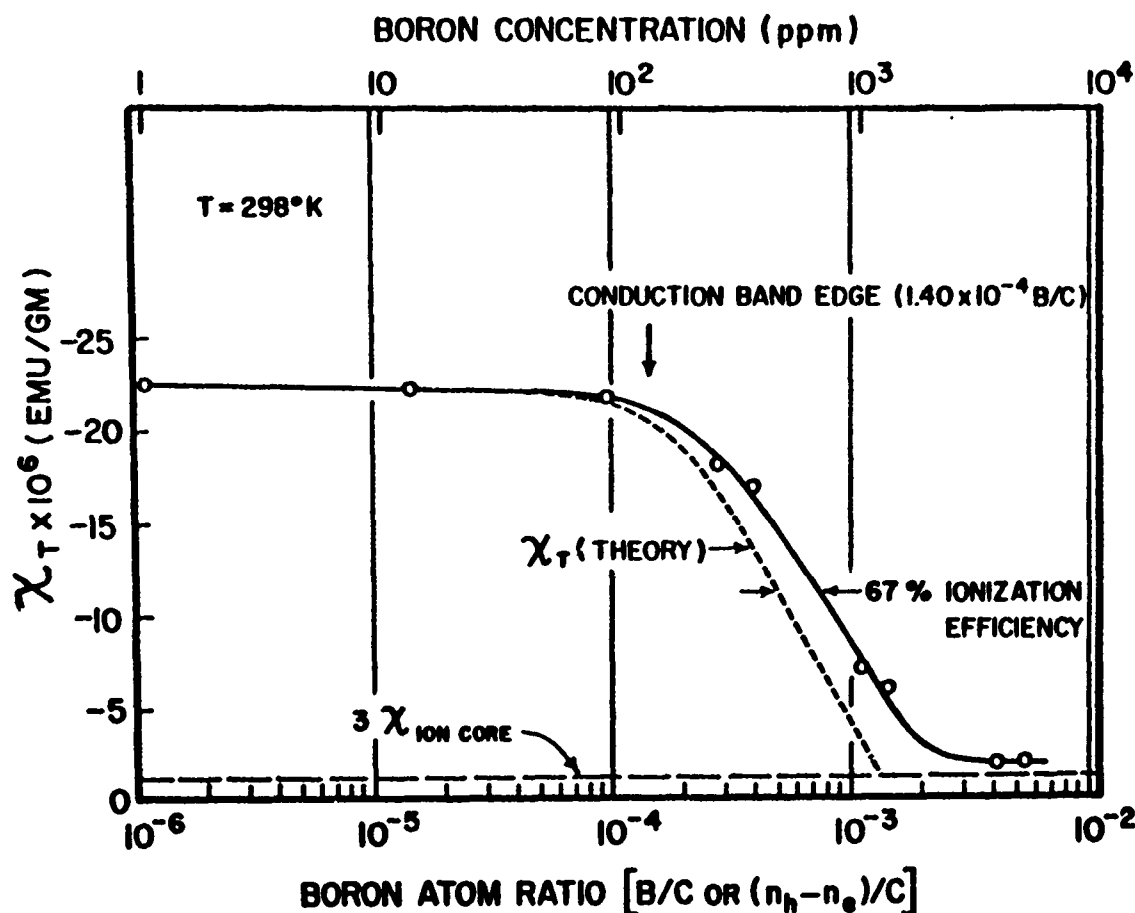
A study has been made of the effect on the electronic properties of graphite due to boron doping. Boron was chosen as a relatively ideal acceptor because of its small size (B^{+3} ion diameter is 0.40 Å) and because it has one fewer valence electron than carbon. There have been indications in the past that the boron atoms go into substitutional trigonal sites in the graphite lattice and in these positions one would expect to obtain close to 100 per cent ionization efficiency. Although heretofore the approach has been indirect, the prime aim here is to study directly the shift of the Fermi level by means of the diamagnetic susceptibility and the change in the actual hole concentration produced by the boron atoms as deduced from the Hall effect.[39] The emphasis is on dilute doping since this produces only a slight perturbation, while maintaining the rigid lattice approximation, from the well established electronic band structure of pure single-crystal graphite. Further, with heavier doping the electron scattering effects, as seen in the electrical conductivity and in the magnetoresistivity, could complicate such a study. It was believed, however, that in this low range their effect would be minimized. Since graphite has a band overlap of about 0.035 ev where the Fermi level lies 0.027 ev above the bottom of the conduction band, one would expect that the shift of the Fermi level due to only a small amount of boron would result in a very pronounced change in the electronic properties, and indeed, this prediction is confirmed.

6.1. Boron Doping Procedure

The boron was introduced by diffusion at 3000°C in an argon atmosphere over a period of one hour. Considerable care was taken in the initial purity of the samples and of the boron itself. Also, considerable attention was devoted to the difficult problem of analyzing the amount of boron that was introduced. Analyses (primarily spectroscopic) from several sources were compared before a value was accepted. The boron concentration values as quoted hereafter are correct within ± 10 per cent. Also, tests were made of the homogeneity of the boron content throughout a given boron level capsule by means of the g-shift in paramagnetic resonance measurements on Madagascar flakes from various parts of the capsule. The values were found to be identical. X-ray measurements[40] showed for the maximum boron concentration of about 0.5 per cent a contraction of 0.043 per cent for the c_o lattice spacing and an expansion of 0.063 per cent for the a_o spacing. In addition, spectroscopic analyses also have supported the fact that during the boronation process only trace amounts of additional impurities were simultaneously introduced.

6.2. Susceptibility Behavior

The results of the susceptibility measurements are seen in Figure 19, where the susceptibility trace is plotted against the boron atom ratio, B/C, the number of boron atoms per carbon atom. The initial trace value for a pure sample starts to drop off with increasing boron concentration in the

BORON CONCENTRATION (ppm)

T = 298°K

CONDUCTION BAND EDGE (1.40×10^{-4} B/C)

χ_T (THEORY)

67 % IONIZATION EFFICIENCY

3 $\chi_{\text{ION CORE}}$

BORON ATOM RATIO $\left[\text{B/C OR } (n_h - n_e)/C\right]$

N-2009

Figure 19. Susceptibility Trace Versus Boron
Concentration for Single Crystals.

neighborhood of 10^{-4} B/C, falling to a low value of -1.9×10^{-6} emu/gm in
the range $\gtrsim 2.5 \times 10^{-3}$ B/C. This susceptibility behavior is directly re-
lated to the rapid negative shift in the Fermi level due to the acceptor
action (see Figure 20), as can be seen from the approximate relation: [13]

$$\chi_c = A \, \frac{\gamma_0^2}{\gamma_1} \int \int \frac{1}{E \left[1 + \exp\left(\frac{E - E_0}{kT}\right)\right] \cos\left(\frac{c_0 k_z}{2}\right)} \, dE \, dk_z \,, \qquad (18)$$

where E = energy and k_z = wave vector in the c-direction. The constants in
this relation are

$$A = \frac{3 a_0^2}{16 \pi^2} \left(\frac{e}{\hbar c}\right)^2 \,,$$

E_0 = Fermi energy, $\gamma_0 \simeq 2.8$ ev and $\gamma_1 \simeq 0.3$ ev. With increasing acceptor
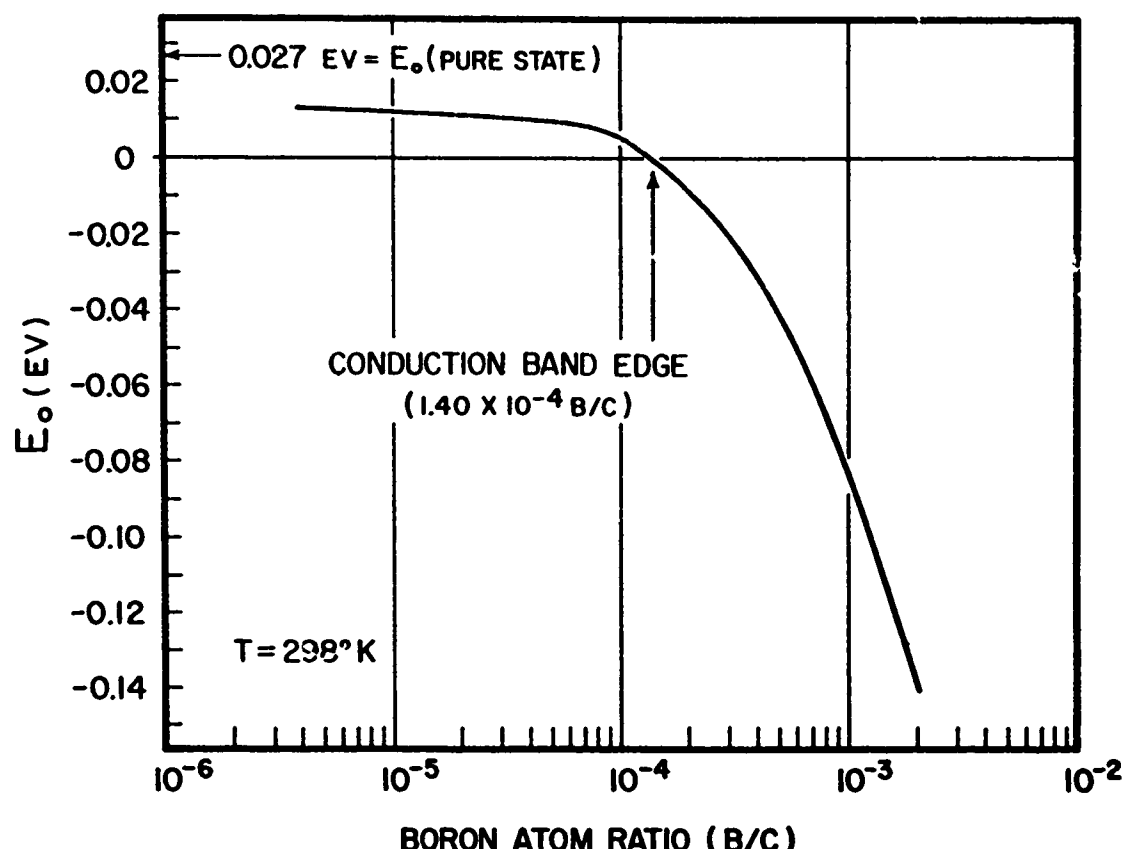
40

Figure 20. Fermi Level Shift Due to Boronation.

doping, χ_c decreases effectively to zero. But from equation (9), χ_T equals $\chi_c + 3\chi_I$, so that the trace then becomes asymptotic to the ionic core component, $3\chi_I$.

The dashed χ_T curve in the figure was calculated from the more exact theory of McClure[13] and normalized along the χ_T axis at the value for pure graphite. The susceptibility trace is plotted versus the number of excess holes per carbon atom, $(n_h - n_e)/C$. By assuming 100 per cent ionization efficiency, the theoretical abscissa coincides with the boron atom ratio abscissa, B/C. It will be seen that the theoretical curve roughly approximates the observed curve. The total drop was contained in the observed $\chi_{||}$ with no change in $\chi_\perp$ with boron concentration. The behavior of $3\chi_I$ is shown as the horizontal dashed line equal to -1.0×10^{-6} emu/gm. The observed asymptotic value is somewhat higher, probably due to the fact that atomic boron inclusions (-0.69×10^{-6} emu/gm) are contributing to the trace at these higher doping levels.

Although qualitatively the experimental and theoretical curves are similar, there is a noticeable shift in the shoulder position. It is believed

41

that this shift results mainly from the fact that 100 per cent ionization efficiency is not attained, as assumed, but rather a somewhat lower efficiency. At one-half height, it will be seen that the difference between these curves gives a value of 67 per cent ionization efficiency.

From the observed susceptibility curve, one can calculate the actual Fermi level shift from the theory (see Figure 20). For pure graphite, the Fermi level lies approximately in the middle of the band overlap region. Upon adding boron, the Fermi level drops, crossing the zero axis at 1.40×10^{-4} B/C. This point then represents the bottom of the conduction band, the point of transition from mixed carrier conduction to hole conduction. With further doping, it continues to drop rapidly so that at 2×10^{-3} B/C its value is about -0.14 ev. The crossover point is indicated in Figure 19 where one may see that it coincides roughly with the initial part of the drop off of the observed susceptibility curve.

6.3 Galvanomagnetic and Transport Properties

Whereas the susceptibility demonstrated the effect due to the drop in the Fermi level, the Hall effect and conductivity measurements show the same effect as manifested in the shift in the concentration of carriers. In addition, the magnetoresistivity and conductivity show the effect of increased electron scattering due to the boron impurity sites. The Hall coefficient behavior, as shown in Figure 21, shows a strong maximum at 2.2×10^{-4} B/C, close to the conduction band edge, at 298°K. This peak shifts to a lower concentration of 3.3×10^{-5} B/C at 77°K. An analysis of this behavior can be made by referring to equation (19), derived from the two-band theory for the low-field Hall coefficient,

$$R_0 = \frac{1}{ec\, n_h} \frac{b^2 - a}{(b + a)^2} \qquad (19)$$

where e is the electronic charge, $a = n_e/n_h$, and $b = \mu_h/\mu_e$. Values for the ratios a and b, as previously determined for the pure case,[23] are

$$a = 1.02$$

and

$$b = 1.15.$$

On the low concentration side of the peak, with increasing boron concentration, the behavior of R_0 is dominated by the increase of $b^2 - a$ as n_h increases compared to n_e. The variation of a dominates since it is a more rapidly varying function than b^2. The peak position, then, corresponds approximately to the concentration where the Fermi level just passes from the mixed carrier region into the single hole conduction region where equation (19) converts to

$$R_0 = \frac{1}{e\, c\, n_h} \qquad (20)$$

Thus, with a further increase of n_h, R_0 decreases on out to the highest concentration observed.
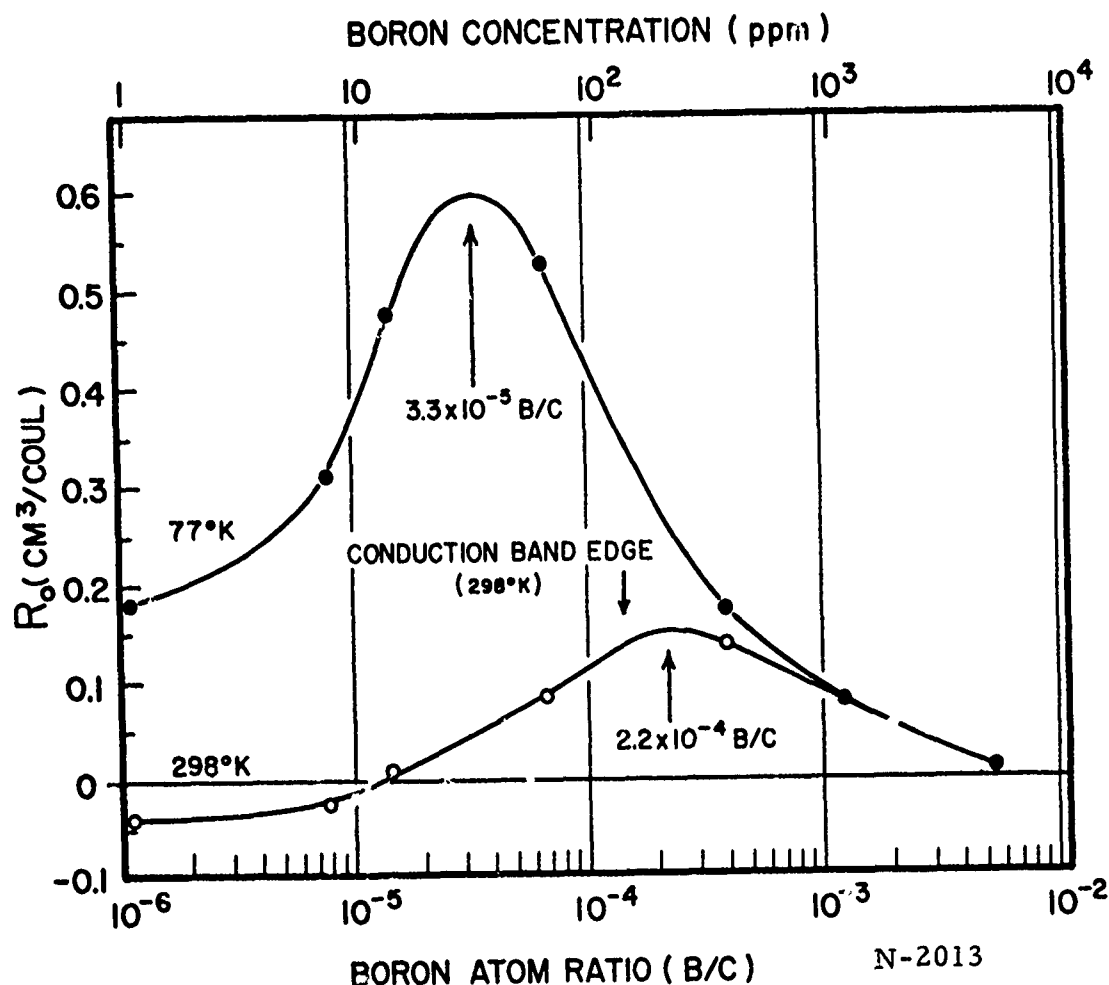
Figure 21. Hall Coefficient Versus Boron Concentration for
Single Crystals at 77°K and 298°K.

Since the Fermi level itself does not shift appreciably with temperature
over this range, the relative position of the peaks is controlled mainly by
the thermal broadening of the Fermi distributions where kT shifts from
0.026 ev at 298°K down to 0.0067 ev at 77°K. Thus, upon going to higher
boron content, the tail of the much broader room temperature distribution
still contributes electrons out to higher concentrations. In fact, Figure 20
shows that the difference in energy of the Fermi level between these two
boron atom ratios is 0.022 ev, approximately equal to the difference in the
above kT values, 0.019 ev. The position of the conduction band edge is
shown also in Figure 21. The exact absolute position of these peaks with
respect to that of the band edge, however, depends on just how the effective
masses and carrier concentrations behave upon approaching and crossing the
bottom of the conduction band. This balance is a delicate one and would re-
quire an extensive analysis to resolve properly. In addition, there could
also be a certain amount of uncertainty in the exact crossover point of the
Fermi level to the extent of the approximation in the susceptibility theory.

The relative height of these peaks (+0.60 cm³/coul at 77°K and +0.15 cm³/coul at 298°K) is controlled primarily by the mobility of the carriers where, in the pure case for instance, the mobility at liquid nitrogen temperature increases roughly by a factor of six over that at room temperature.[23]

The behaviors of the electrical conductivity and the magnetoresistivity with boron atom ratio are shown in Figure 22. The points at 1 ppm B are the
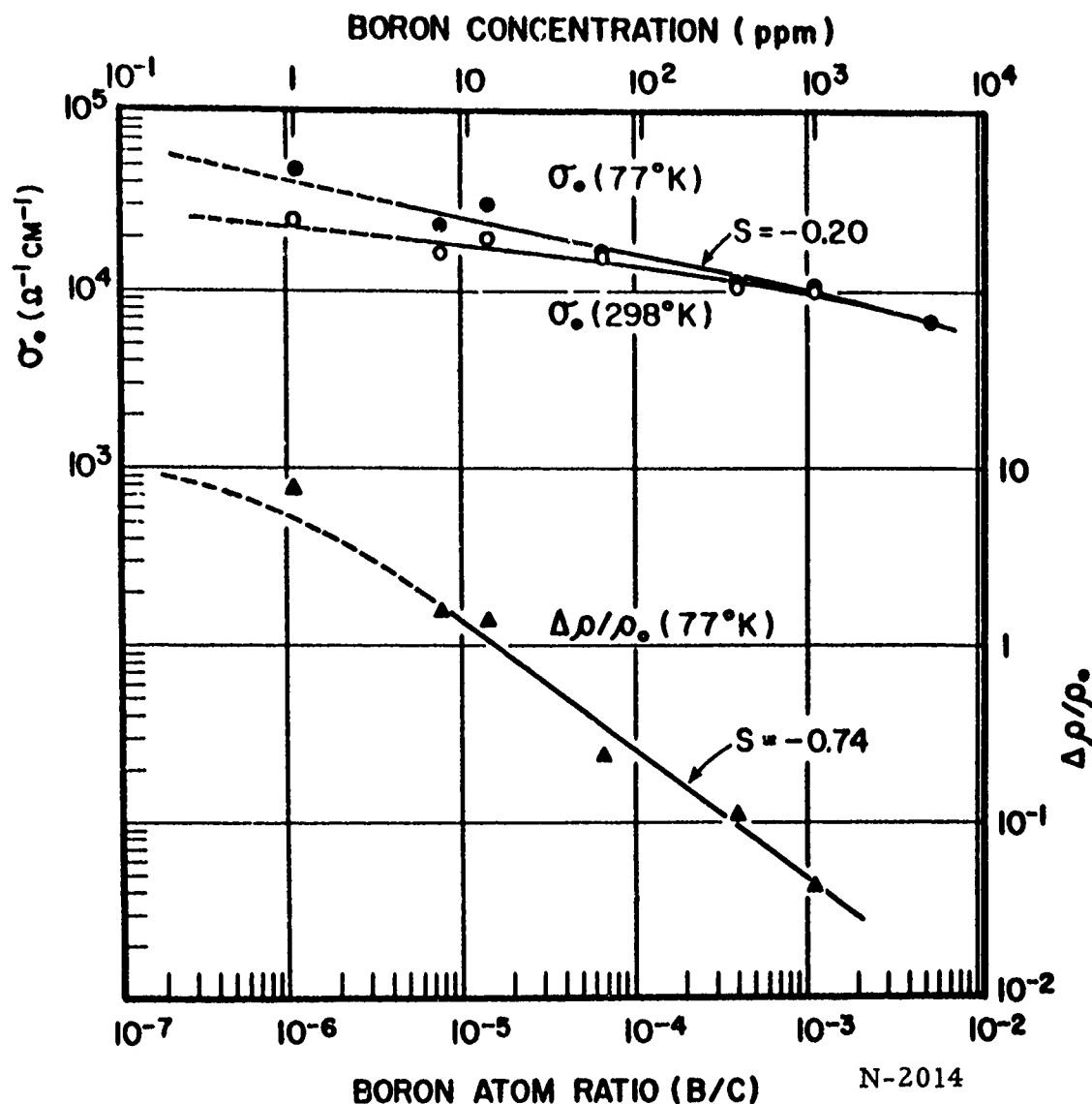
BORON CONCENTRATION (ppm)

Figure 22. Electrical Conductivity and Magnetoresistivity Versus Boron Concentration.

values measured previously on a pure crystal where the exact boron concentration was known only to be in the range ≤ 1 ppm. Both the conductivity and

magnetoresistivity decrease with boronation. In the case of the conductivity, the slope is -0.20. The sign of this slope is controlled by the dominance of the increased scattering of the boron atoms over that of the increased number of holes introduced. This behavior is opposite to that of polycrystalline graphite,[41] probably resulting from the fact that here the resultant mobility is of the order of 10^5 cm^2/v sec and is much more sensitive to a given introduction of scattering centers than in the polycrystalline case where the presence of scattering centers in the original material has already reduced the mobility to the order of 10^3 cm^2/v sec. Thus, the scattering due to an additional relatively small number of boron atoms would make little difference.

The magnetoresistivity, taken at 3.94 kilogauss, decreases at a more rapid rate (slope = -0.74), since it does not have the compensating influence of the increasing hole concentration. While not precisely the lowest-field case where the H^2 dependence is followed over the whole temperature range, the magnetoresistance variation as a function of boronation gives a general idea of the behavior of the mobilities involved. In the mixed-carrier region, $\Delta\rho/\rho_0$ is proportional to $\mu_e \mu_h$. It is interesting to note (see Figure 23) that the hole Hall mobility ($\mu_h = R_0 \sigma_0$) in the shoulder region between 10^{-4} and 10^{-3} B/C is proportional to $B^{-0.86}$. This slope is equal to the square root of the absolute value of the magnetoresistivity slope, $|-0.74|$, indicating a mobility-square dependence even in this single-carrier region.

The hole carrier concentration is shown at the top part of the curve as determined from equation (20) for the Hall effect. From this information, another determination of ionization efficiency can be made. If the equivalent position where the ionization efficiency was taken on the susceptibility curve giving 67 per cent is taken here, a value of 75 per cent is obtained. Actually, a range of ionization efficiencies was observed over the concentration range of the shoulder in both of these determinations. For instance, in the case of the susceptibility, at the band edge a value of 80 per cent was found decreasing to a value of 65 per cent at 1.44×10^{-3} B/C. A similar range was found from the Hall effect. It must be kept in mind, however, that this efficiency still is not quite the true efficiency that might be expected from an atom definitely known to be in a trigonal site. Since a certain percentage of the boron atoms becomes trapped in imperfection sites of various types, they could be rendered ineffective toward shifting the Fermi level.

In the high boron concentration region (B/C $\gtrsim 10^{-3}$), both the Hall coefficient and conductivity become independent of temperature as shown in Figures 21 and 22. Since μ_h becomes independent of temperature, it is believed that scattering from these ionized boron centers dominates over the lattice scattering. The independence of n_h with temperature, on the other hand, is apparently not so straightforward. It is postulated that these impurity levels are distributed over a range of energy located near the band edge since even down as far as -0.1 ev ($\sim$ 4kT), holes are still being introduced. The exact character and distribution of these impurity states would necessitate further extensive investigation.
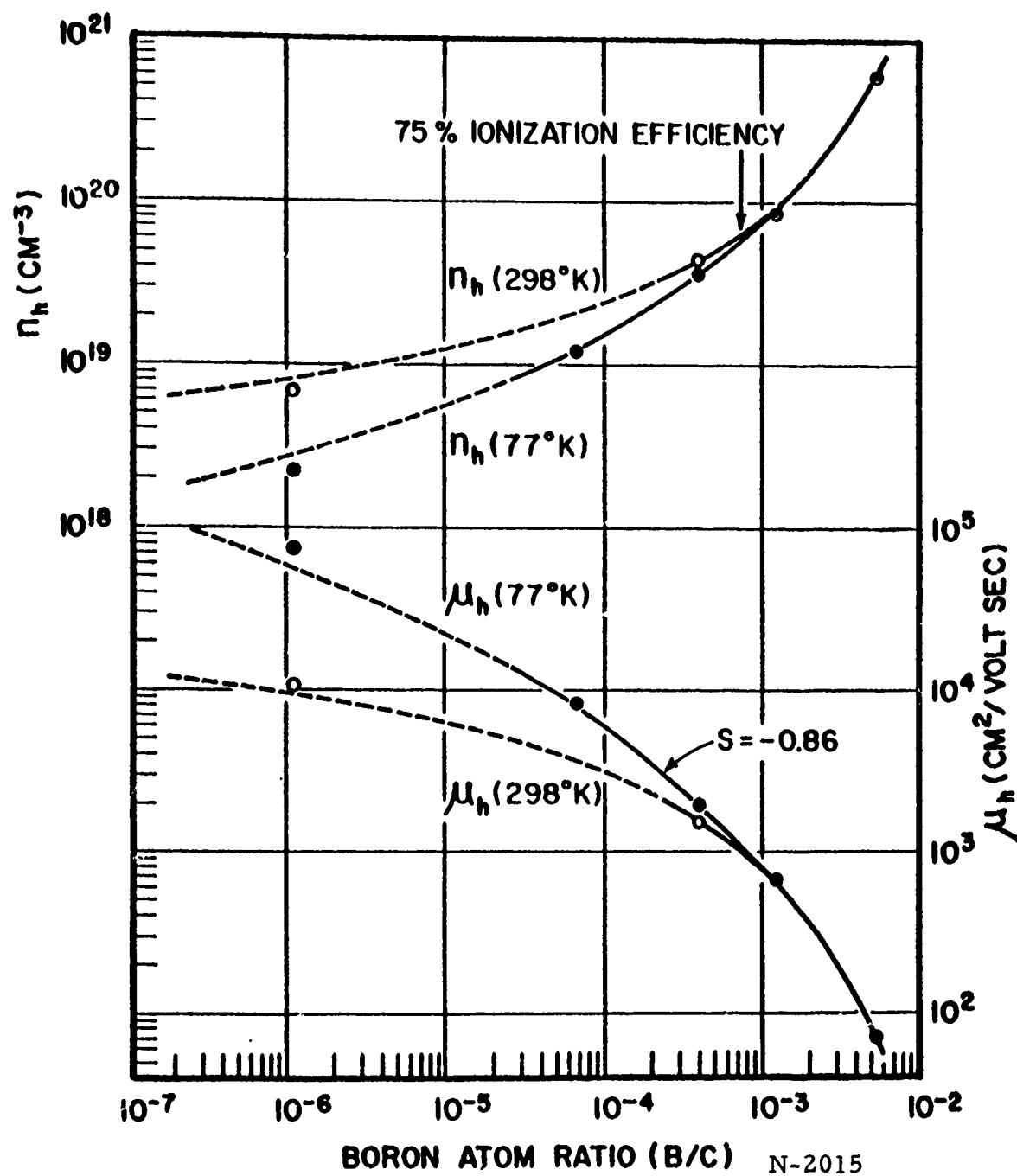
45

Figure 23. Hall Mobility and Concentration of Holes
Versus Boron Concentration at 77°K
and 298°K.

46

7. REFERENCES

1. C. A. Hutchison, Phys. Rev., 75, 465 (1949).

2. L. F. Bates, Modern Magnetism (Cambridge Univ. Press, 1951), p. 157.

3. J. J. Donoghue, NAA-SR-117 (1953).

4. N. Davy, Phil. Mag., 33, 575 (1942).

5. A. W. Czanderna and J. M. Honig, Analytical Chemistry, 29, 1206 (1957).

6. Reference 2, p. 289.

7. K. Honda, Ann. der Phys., 32, 1027 (1910).

8. M. Owen, Ann. der Phys., 37, 657 (1912).

9. W. G. Henry and J. L. Rogers, Phil. Mag., 1, 223 (1956).

10. M. Garber, W. G. Henry and N. G. Hoeve, Can. Jour. Phys., 38, 1595 (1960).

11. E. W. Pugh and F. M. Ryan, Phys. Rev., 111, 1038 (1958).

12. Y. Shimizu, Sci. Rep. Tohoku Univ., 25, 921 (1937).

13. J. W. McClure, Phys. Rev., 119, 606 (1960).

14. W. Primak and L. H. Fuchs, Phys. Rev., 95, 22 (1954); W. Primak, Phys. Rev., 103, 544 (1956).

15. H. Lipson and A. R. Stokes, Proc. Roy. Soc., 181A, 101 (1942).

16. A. Pacault, A. Marchand, F. Boy and E. Poquet, Comp. Rendus, 254, 1275 (1962); and A. Marchand, A. Pacault and A. Forchioni, Comp. Rendus, 255, 1257 (1962).

17. G. E. Bacon, Acta Cryst., 3, 320 (1950).

18. J. W. McClure, National Carbon Research Laboratory, Monthly Report, July 1, 1962.

19. H. Honda, Proc. of Third Conf. on Carbon, Pergamon Press (1959), p. 159; and A. Pacault and A. Marchand, Jour. Chim. Phys., 57, 873 (1960).

20. H. T. Pinnick, Phys. Rev., 94, 319 (1954) and A. F. Adamson and H. E. Blayden, Proc. of Third Conf. on Carbon, Pergamon Press (1959), p. 147.

21. D. E. Soule, National Carbon Research Laboratory, Biweekly Report, Dec. 24, 1954; Monthly Report, March 15, 1957.

22. E. Poquet, N. Lumbroso, J. Hoarau, A. Marchand, A. Pacault and D. E. Soule, Jour. Chim. Phys., $\underline{57}$, 866 (1960).

23. D. E. Soule, Phys. Rev., $\underline{112}$, 698 (1958) and C. Palache, Amer. Mineralogist, $\underline{26}$, 709 (1941).

24. C. S. Smith, Solid State Physics, Acad. Press, Inc., New York (1958), Vol. 6, p. 192.

25. A. Pacault, J. Hoarau, J. Joussot-Dubien, B. Demanceau and N. Lumbroso, Proc. of Third Conf. on Carbon, Pergamon Press (1959), p. 43.

26. K. S. Krishnan, Nature, $\underline{133}$, 174 (1934).

27. I. I. Rabi, Phys. Rev., $\underline{29}$, 174 (1927).

28. K. Honda and T. Sonĕ, Scientific Reports, Tohoku Imp. Univ., $\underline{2}$, 25 (1913).

29. B. C. Guha and B. P. Roy, Indian Jour. Phys., $\underline{8}$, 345 (1934).

30. K. S. Krishnan and N. Ganguli, Zeits. Krist., $\underline{A100}$, 530 (1939).

31. J. J. Donoghue and J. D. McClelland, NAA-SR-153 (1951).

32. W. P. Eatherly and J. D. McClelland, Phys. Rev. (L), $\underline{89}$, 661 (1953).

33. G. B. Spence, as reported in WADD Technical Report 61-72, Volume XLII, Summary Technical Report, p. 44-47.

34. R. L. Finicle, as reported in WADD Technical Report 61-72, Volume XXXVII, Studies of Graphite Deposited by Pyrolytic Processes, by P. H. Higgs, R. L. Finicle, R. J. Bobka, E. J. Seldin, and K. I. Zeitsch.

35. R. Franklin, Acta. Crys., $\underline{4}$, 253 (1951).

36. D. B. Fischbach, Phys. Rev., $\underline{123}$, 1613 (1961).

37. WADD Technical Report 61-72, Volume XX, The Electric and Magnetic Properties of Pyrolytic Graphite, by G. Wagoner and B. H. Eckstein.

38. J. T. Meers, unpublished data, National Carbon Company Research Laboratories, ERC-348 (1955).

39. Hall effect, magnetoresistivity, and conductivity results along with the susceptibility have been discussed in detail previously (D. E. Soule, Proc. of Fifth Conf. on Carbon, Pergamon Press [1962], Volume I, p. 13).

40. C. E. Lowell, private communication.

41. A. Ubbelohde, Proc. of Fifth Conf. on Carbon, Pergamon Press (1962), Volume I, p. 1.